

# $\gamma$ -Alumina: The Essential and Unexpected Role of Water for the Structure, Stability, and Reactivity of “Defect” Sites

Raphael Wischert,<sup>†,‡,§</sup> Pierre Laurent,<sup>†</sup> Christophe Copéret,<sup>\*,†,‡</sup> Françoise Delbecq,<sup>§</sup> and Philippe Sautet<sup>\*,§</sup>

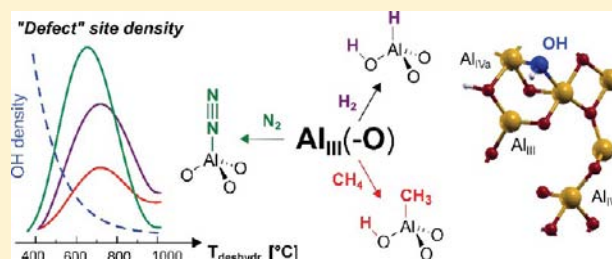
<sup>†</sup>Université de Lyon, CNRS, Institut de Chimie de Lyon, C2P2, CPE Lyon, 43, Bd. du 11 Novembre 1918, F-69616 Villeurbanne Cedex (France)

<sup>‡</sup>Department of Chemistry, ETH Zürich, Wolfgang Pauli Strasse 10, CH-8093 Zürich (Switzerland)

<sup>§</sup>Université de Lyon, CNRS, Institut de Chimie de Lyon, École Normale Supérieure de Lyon, 46 allée d'Italie, F-69364 Lyon Cedex 07 (France)

## S Supporting Information

**ABSTRACT:** Combining experiments and DFT calculations, we show that tricoordinate  $\text{Al}_{\text{III}}$  Lewis acid sites, which are present as metastable species exclusively on the major (110) termination of  $\gamma$ - and  $\delta$ - $\text{Al}_2\text{O}_3$  particles, correspond to the “defect” sites, which are held responsible for the unique properties of “activated” (thermally pretreated) alumina. These “defects” are, in fact, largely responsible for the adsorption of  $\text{N}_2$  and the splitting of  $\text{CH}_4$  and  $\text{H}_2$ . In contrast, five-coordinate Al surface sites of the minor (100) termination cannot account for the observed reactivity. The  $\text{Al}_{\text{III}}$  sites, which are formed upon partial



dehydroxylation of the surface (the optimal pretreatment temperature being 700 °C for all probes), can coordinate  $\text{N}_2$  selectively. In combination with specific O atoms, they form extremely reactive  $\text{Al}_2\text{O}$  Lewis acid–base pairs that trigger the low-temperature heterolytic splitting of  $\text{CH}_4$  and  $\text{H}_2$  to yield  $\text{Al}-\text{CH}_3$  and  $\text{Al}-\text{H}$  species, respectively.  $\text{H}_2$  is found overall more reactive than  $\text{CH}_4$  because of its higher acidity, hence it also reacts on four-coordinate sites of the (110) termination. Water has the dual role of stabilizing the (110) termination and modifying (often increasing) both the Lewis acidity of the aluminum and the basicity of nearby oxygens, hence the high reactivity of partially dehydroxylated alumina surfaces. In addition, we demonstrate that the presence of water enhances the acidity of certain four-coordinate Al atoms, which leads to strong coordination of the CO molecule with a spectroscopic signature similar to that on  $\text{Al}_{\text{III}}$  sites, thus showing the limits of this widely used probe for the acidity of oxides. Overall, the dual role of water translates into optimal water coverage, and this probably explains why in many catalyst preparations, optimal pretreatment temperatures are typically observed in the “activation” step of alumina.

## ■ INTRODUCTION

Transition aluminas ( $\text{Al}_2\text{O}_3$ ), also known as “activated aluminas”, are generated by thermal treatment of alumina precursors (most commonly aluminum hydroxides) at temperatures below ca. 800 °C, thus preventing the formation of the thermodynamically most stable but low surface  $\alpha$ - $\text{Al}_2\text{O}_3$  (corundum). These high-surface materials are known as  $\gamma$ -,  $\delta$ -,  $\kappa$ -,  $\chi$ -, or  $\eta$ - $\text{Al}_2\text{O}_3$ , depending on the nature of the precursor and the synthesis process.<sup>1–4</sup>

They are among the most widely used oxides in heterogeneous catalysis, especially for the petroleum industry, and they find applications as catalyst supports for (noble) metals in a variety of processes, where they often play an essential role by contributing to catalytic activity and stability.<sup>5</sup> Notable applications involve hydrotreating operations, such as desulfurization (Co–Mo, Ni–Mo/ $\text{Al}_2\text{O}_3$ ), catalytic dehydration of n-butanol for rubber production ( $\text{Cr}_2\text{O}_3/\text{Al}_2\text{O}_3$ ),<sup>2</sup>

methanol synthesis (Cu/Zn/ $\text{Al}_2\text{O}_3$ ), and their use as washcoat in exhaust gas catalytic converters (Pt,Pd,Rh/ $\text{Al}_2\text{O}_3$ ).<sup>6</sup>

Transition aluminas are also a key component of highly active single-site supported systems<sup>7–9</sup> for hydrogenation,<sup>10</sup> polymerization,<sup>11–14</sup> or metathesis of alkenes.<sup>15,16</sup> For example,  $\text{CH}_3\text{ReO}_3$  supported on  $\gamma$ -alumina<sup>17–19</sup> affords highly active alkene metathesis catalysts, while it leads to an inactive system when supported on  $\text{SiO}_2$ .<sup>17</sup> The alumina support has also been shown to be essential for the stabilization and formation of highly reactive W<sup>–20–22</sup> and Zr–hydride<sup>23</sup> species, which catalyze the conversion of alkanes into higher homologues (alkane metathesis).

Alumina itself can also play the role of a catalyst, for instance in alcohol dehydration or in the Claus process for sulfur removal from gases; the latter being the largest application of

Received: May 2, 2012

Published: August 3, 2012

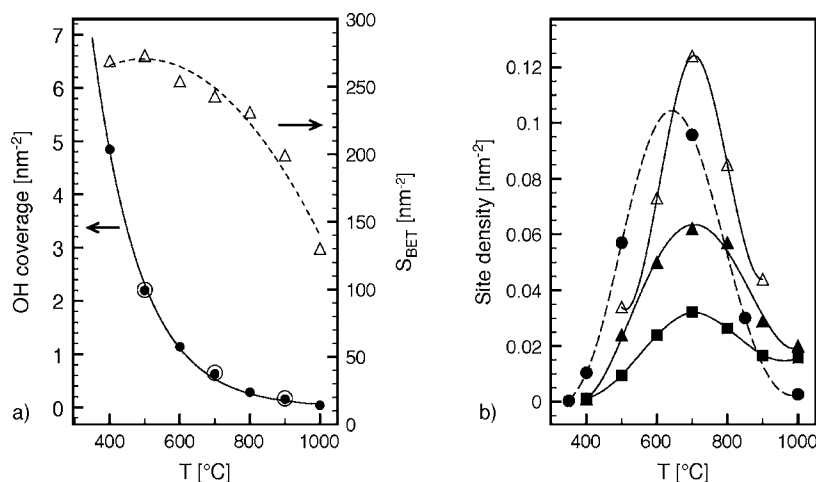


**Figure 1.** (a) Evolution of the hydroxyl coverage on  $\gamma$ -Al<sub>2</sub>O<sub>3</sub> (SBA-200), as a function of its pretreatment temperature, measured by titration with CH<sub>3</sub>MgBr (larger empty circles) or by integration of the OH bands in the IR spectrum (●, the OH-density scale (Y) is based on titration; see the corresponding spectra in Figure S1). Surface area as of  $\gamma$ -Al<sub>2</sub>O<sub>3</sub> as a function of pretreatment temperature measured by N<sub>2</sub> adsorption ( $\Delta$ ). (b) Al-X (X = CH<sub>3</sub>, H, N<sub>2</sub>) site density (nm<sup>-2</sup>, arbitrary unit in case of N<sub>2</sub>) as a function of the pretreatment temperature of  $\gamma$ -Al<sub>2</sub>O<sub>3</sub>: ■, CH<sub>4</sub>, reaction temperature 150 °C; ▲, H<sub>2</sub>, reaction temperature 25 °C;  $\Delta$ , H<sub>2</sub>, reaction temperature 150 °C; --●--, N<sub>2</sub>, adsorption temperature 25 °C (on  $\gamma/\delta$ -Al<sub>2</sub>O<sub>3</sub>). For N<sub>2</sub>, no absolute site density was measured; the data points are scaled by an arbitrary constant factor to fit within the values obtained for H<sub>2</sub> and CH<sub>4</sub>.

this oxide as a catalyst itself<sup>2</sup> and the largest source of elemental sulfur.

One of the most striking and unexpected properties of transition aluminas is that they catalyze at low-temperature reactions involving the dissociation of H–H and C–H bonds. Already in the 1950–1960s it was reported that alumina pretreated at high temperature catalyze the ortho- to para-H<sub>2</sub> conversion<sup>24,25</sup> and H–D exchange reactions.<sup>24–30</sup> Reactions involving the dissociation of C–H bonds, such as the H–D exchange of methane,<sup>31–33</sup> alkanes,<sup>34,35</sup> alkenes,<sup>36</sup> and benzene,<sup>37</sup> the double-bond isomerization of alkenes<sup>36</sup> and the cis/trans isomerization of alkenes typically occur at room temperature. The activation of C–C bonds, for example, in the skeletal isomerization of alkenes requires higher temperatures (above 300 °C).<sup>1</sup>

All these reactions have been associated to a small number of active sites, so-called “defect sites” or  $\alpha$ -sites,<sup>38</sup> i.e., coordinatively unsaturated (“cus”) Lewis acidic Al and Lewis basic O surface atoms.<sup>1</sup> However, the precise nature and structure of these surface active sites have largely remained unclear until now. The reactivity of surface atoms is usually correlated with their coordination number, the lowest coordination being associated to the highest acidity or basicity. We have shown that the tricoordinate Al<sub>III</sub> Lewis acid sites present on the (110) surface readily coordinate N<sub>2</sub><sup>39</sup> and are highly reactive in the heterolytic splitting of the H–H bond of H<sub>2</sub> and the C–H bond of CH<sub>4</sub>.<sup>40</sup> These studies were based on experimental data as well as calculations focused on the fully dehydrated major (110) termination as a model for the reactive  $\gamma$ -alumina surface; this facet being the only one exposing Al<sub>III</sub>. The reaction of H<sub>2</sub> and CH<sub>4</sub> leads to the formation of O–H and Al–X (H/CH<sub>3</sub>), showing that O atoms are also involved in the adsorption process. However this fully dehydrated (110) termination does not exist in real conditions since it would require pretreatment temperatures above the stability limit of  $\gamma$ -alumina. More recently, in the specific case of CH<sub>4</sub>, we have also shown that the presence of water on the surface of alumina can lead to the generation of highly reactive “frustrated” Al<sub>III</sub>O Lewis acid–base pairs, which facilitate the heterolytic splitting

of methane at optimal water coverage. We found a volcano-type behavior for the adsorption site density as a function of pretreatment temperature of alumina, with a maximum at 700 °C.<sup>41</sup>

These findings clearly ask for a more general understanding of the surface reactivity of alumina as a function of the hydration level: What are the potential surface sites, and how are they affected by partial hydration? Is the adsorption of various probe molecules (dissociative and nondissociative) affected in the same way by hydration? Are tricoordinate Al<sub>III</sub> sites responsible for the adsorption of all these probe molecules (CH<sub>4</sub>, H<sub>2</sub>, and N<sub>2</sub>)? Can one intuitively predict the reactivity of a site solely based on local structural parameters, such as coordination?

Using a combined theoretical and experimental approach, we investigate the structure of Al and O Lewis acid and base sites on the major (110) and minor (100) terminations of  $\gamma$ -Al<sub>2</sub>O<sub>3</sub> for various hydroxyl concentrations, including metastable structures with lower existence probability, which are associated with high reactivity. We then study the Lewis acidity of these surfaces as a function of partial hydroxylation, by monitoring the coordination of N<sub>2</sub> to surface sites through infrared (IR) spectroscopy. These experiments are compared with calculated adsorption energies and frequency shifts. Additional calculations are carried out on the adsorption of the CO molecule, one of the most widely used probes for Lewis acid sites on oxides. Finally, we compare the C–H and H–H bond dissociation of CH<sub>4</sub> or H<sub>2</sub> as a function of pretreatment temperature of alumina and hence of hydroxyl coverage, in this case probing both the Lewis acid Al and basic O sites. We show that the reactivity of Al and O sites is affected in a counterintuitive way by partial hydroxylation and that atomic coordination is not a complete descriptor of reactivity. In addition, we rationalize the similarities and differences in the reactivity of CH<sub>4</sub> and H<sub>2</sub>.

## ■ EXPERIMENTAL RESULTS

**Remarks on the Aluminas Used in the Study.** We carried out experiments on a boehmite-derived  $\gamma$ -Al<sub>2</sub>O<sub>3</sub> (SASOL SBA-200) with a specific surface area of ca. 250 m<sup>2</sup> g<sup>-1</sup> and a pyrogenic  $\gamma/\delta$ -Al<sub>2</sub>O<sub>3</sub> (Evonik/Degussa Alu C) with a specific surface area of ca. 120 m<sup>2</sup> g<sup>-1</sup>. The  $\gamma$ - and  $\delta$ -phase can be considered structurally very similar but with a higher degree of cation ordering in the latter (see Gribov et al. and references therein).<sup>42</sup> XRD shows indeed a higher degree of crystallinity for Degussa C [see Figure S3 and discussion of XRD in the Supporting Information (SI)]. On both transition aluminas the (110) termination dominates largely (ca. 80% of the particle surface) over the (100) and (111) facets.<sup>42–46</sup> More exhaustive information regarding the experiments can be found in the SI.

**Evolution of the OH Density and Structure of Al<sub>2</sub>O<sub>3</sub> as a Function of Pretreatment Temperature.** After calcination at 500 °C, the alumina samples were pretreated at temperatures between 400 and 1000 °C. Within this temperature range the density of OH groups, measured by titration with CH<sub>3</sub>MgBr and by integration of the OH-bands of the IR spectrum (see Figure 1a and Figure S1), decays in an almost exponential fashion vs the pretreatment temperature.<sup>41</sup>

The dehydroxylation process is associated with a sudden drop (ca. 50%) of the specific surface area above 800 °C, as evaluated by nitrogen adsorption (Figure 1a), and it parallels the transformation of alumina from  $\gamma$  into the  $\delta$ - and  $\theta$ -phases as evidenced by XRD (see Figures S2 and S3 and also similar data from the literature).<sup>4,47</sup>

**Evaluation of the Reactive Sites Density by N<sub>2</sub>.** The adsorption of dinitrogen (N<sub>2</sub>) on  $\gamma/\delta$ -Al<sub>2</sub>O<sub>3</sub> (Degussa Alu C)<sup>48</sup> was monitored by transmission IR spectroscopy because it gives rise to a single, sharp band centered at 2355 cm<sup>-1</sup>, attributed to the N–N stretching vibration of N<sub>2</sub> adsorbed on highly Lewis acidic tricoordinate Al<sub>III</sub> sites of Al<sub>2</sub>O<sub>3</sub> (Figure S4).<sup>39</sup> The intensity/integral of this band as a function of pretreatment temperature describes a volcano curve starting at ca. 400 °C, with a maximum at ca. 700 °C and then a decreasing site density for higher pretreatment temperatures of alumina (Figure 1b). Note that the position of both the center of the band and the residual rotational bands does not change, indicating that N<sub>2</sub> adsorbs on one single type of site and that it is not the strength of the site but its amount that varies with pretreatment temperature.

**Titration of Reactive Sites for Methane Dissociation.** Methane reacts at 150 °C with the surface of  $\gamma$ -Al<sub>2</sub>O<sub>3</sub> to generate surface OH groups and Al–CH<sub>3</sub>; the reactive sites can be titrated upon hydrolysis by measuring the amount of methane released. As found for N<sub>2</sub> and reported earlier by us,<sup>41</sup> the density of sites follows a volcano curve (Figure 1b), with a maximum of 0.03 sites nm<sup>-2</sup> at ca. 700 °C. The experiments carried out on Degussa C ( $\gamma/\delta$ -Al<sub>2</sub>O<sub>3</sub>) show the exact same volcano-type behavior, but the site density is higher by ca. 10–20% than on SBA-200 (Figure S5). This suggests that sites of similar reactivity are located on  $\gamma$ - and  $\delta$ -Al<sub>2</sub>O<sub>3</sub> and that they are preferentially located on crystalline domains, because Degussa C has a higher degree of crystallinity than SBA-200.

**Titration of Reactive Sites for Dihydrogen Dissociation.** The reaction of H<sub>2</sub> with  $\gamma$ -Al<sub>2</sub>O<sub>3</sub> was first carried out at a reaction temperature of 25 °C (Figure 1b), and the Al–H sites titrated upon hydrolysis. As in the case of CH<sub>4</sub>, the number of sites dissociating H<sub>2</sub> describes a volcano curve with a maximum at 700 °C. Note that the number of sites capable of dissociating

H<sub>2</sub> is ca. twice higher than for CH<sub>4</sub>, even if the reaction temperature is 150 °C for CH<sub>4</sub> vs 25 °C for H<sub>2</sub>. In fact, titration of Al–H at 150 °C yields an even higher density of sites, reaching 0.13 nm<sup>-2</sup> at 700 °C. Again, additional experiments on Degussa C alumina show the same volcano curve but a higher site density for a given pretreatment temperature of alumina (Figure S5).

The salient feature of these adsorption experiments is clearly the volcano-type behavior of the adsorption site density as a function of the pretreatment temperature, independent of the probe and the adsorption mode, dissociative for H<sub>2</sub> and CH<sub>4</sub> on Al<sub>III</sub>O sites or nondissociative (coordination) for N<sub>2</sub> on Al sites. This indicates that similar sites must be involved in the adsorption of CH<sub>4</sub>, H<sub>2</sub>, and N<sub>2</sub>. These sites are generated at pretreatment temperatures above 400 °C and reach a maximum density at 700 °C, i.e., where the alumina surface is still hydrated to a significant extent (ca. 0.7 OH nm<sup>-2</sup>). Although one would expect that the highest reactivity is associated with a total removal of adsorbed water, thus liberating a maximum of highly reactive Al<sub>III</sub>O sites, a different scenario is observed: a significant drop of the site density for pretreatment temperatures above 700 °C, which is concomitant with the drop of the surface area and the transformation of the alumina phase from  $\gamma/\delta$  to  $\theta$ . Additionally, despite the same overall volcano curve for all probes, it is noteworthy that the density of Al–H sites is always higher than that of Al–CH<sub>3</sub> sites, even when comparing the adsorption of H<sub>2</sub> at 25 °C with that of CH<sub>4</sub> at 150 °C. This implies that CH<sub>4</sub> reacts only on the most reactive sites, while H<sub>2</sub> is also dissociated on less reactive ones.

## ■ QUANTUM CHEMICAL MODELING OF ALUMINA SURFACES

**Realistic Models of Alumina Surfaces.** For the description of  $\gamma$ -Al<sub>2</sub>O<sub>3</sub> we use a model with nonspinel sites occupied, based on the simulated dehydration of boehmite.<sup>49,50</sup> DFT calculations in periodic boundary conditions are carried out in the Perdew–Wang (PW91) implementation<sup>51</sup> of the generalized gradient approximation (GGA) for the correlation and exchange energy functional, using the VASP code (version 4.6).<sup>52,53</sup> The projected augmented wave (PAW)<sup>54</sup> method was adopted for describing the electron–ion interactions. The climbing image nudged elastic band method (CI-NEB)<sup>55,56</sup> was used to determine the transition states (TSs). More details are reported in the SI.

The bulk of  $\gamma$ -Al<sub>2</sub>O<sub>3</sub> consists of aluminum ions in tetrahedral (25%) and octahedral (75%) coordination.<sup>49</sup> The unit cell of the most abundant (110) termination (ca. 80%) exposes one tricoordinate Al<sub>III</sub> and two types of tetracoordinate Al<sub>IV</sub> sites, namely Al<sub>IVa</sub> and Al<sub>IVb</sub> (**s0**, Figure 2a), resulting from tetrahedral and octahedral bulk Al atoms, respectively, while the less abundant (100) termination (ca. 10%) exposes only Al<sub>V</sub> sites (Al<sub>Va</sub>–Al<sub>Vd</sub>, Figure 2b).

However, this bare (110) termination with low-coordinated Al cannot be considered as a realistic model for  $\gamma$ -Al<sub>2</sub>O<sub>3</sub> surfaces because the surface sites are partially occupied by OH groups or protons, since complete dehydration is not reached on that surface at usual pretreatment temperature.

Thermodynamic calculations show that the surface energy of the fully dehydrated (110) termination is higher (less stable) than that of the (100) surface.<sup>50,57</sup> The bare (110) facet is therefore metastable but strongly stabilized by hydroxylation, and calculations predict its full dehydration only at high temperature, around 900 °C, in agreement with experiment

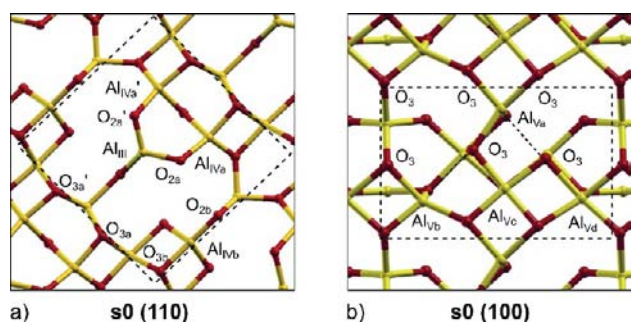


**Figure 2.** (a) Fully dehydroxylated (110) termination of  $\gamma$ - $\text{Al}_2\text{O}_3$  ( $s_0$ ), and (b) fully dehydroxylated (100) termination. Only the top two layers of the periodical slab are represented. A dashed line indicates the unit cell; Al, yellow; O, red.

which shows that this is achieved at around 1000 °C (Figure 1a), a temperature well above the stability domain of the  $\gamma$ -phase. In contrast, the intrinsically more stable (100) termination is free of water at much lower temperatures (ca. 350 °C). We will therefore study the reactivity of the (100) termination in the fully dehydrated state and that of the (110) termination at different levels of hydration. Note that the polar

(111) termination is present to a smaller extent (ca. 10%) on  $\gamma$ - $\text{Al}_2\text{O}_3$  particles. We do not consider this facet because it exposes only oxygen atoms and because its dehydroxylation demands very high temperatures.

**Adsorption of Water on the (110) Termination.** Water strongly adsorbs on the most abundant (110) termination of  $\gamma$ - $\text{Al}_2\text{O}_3$ . To reproduce the experimentally observed water coverage in the investigated range of pretreatment temperatures (400–1000 °C), OH coverages of 3, 6, and 9 OH  $\text{nm}^{-2}$  were simulated, corresponding to 1, 2, and 3  $\text{H}_2\text{O}$  per unit cell and referred to as  $s_1$ ,  $s_2$ , and  $s_3$  surfaces, respectively (Figure 3, Table 1, and Figure S6). Compared to previous work<sup>50</sup> we have investigated a comprehensive range of surface structures for each water coverage, including low-energy metastable isomers. Surfaces “ $s_{ia}$ ” (and isomers  $s_{ia}'$ ,  $s_{ia}''$ , etc.) have  $\text{Al}_{\text{III}}$  occupied by an OH group and correspond in general to the most stable configurations at a given OH coverage. Surfaces “ $s_{ib}$ ” are other low-energy isomers, while surfaces “ $s_{ic}$ ” always expose a free  $\text{Al}_{\text{III}}$  site.

**Low Water Coverage (3 OH  $\text{nm}^{-2}$ ).** Adsorption of one water molecule on the  $\text{Al}_{\text{III}}$  site of the bare  $s_0$  surface is highly exoenergetic, with  $E_{\text{ads}}(\text{H}_2\text{O}) = -226 \text{ kJ mol}^{-1}$ .  $\text{H}_2\text{O}$  is dissociated on  $\text{Al}_{\text{III}}\text{O}_{2a}$  yielding a terminal OH ( $\text{Al}_{\text{IV}}\text{OH}$ )

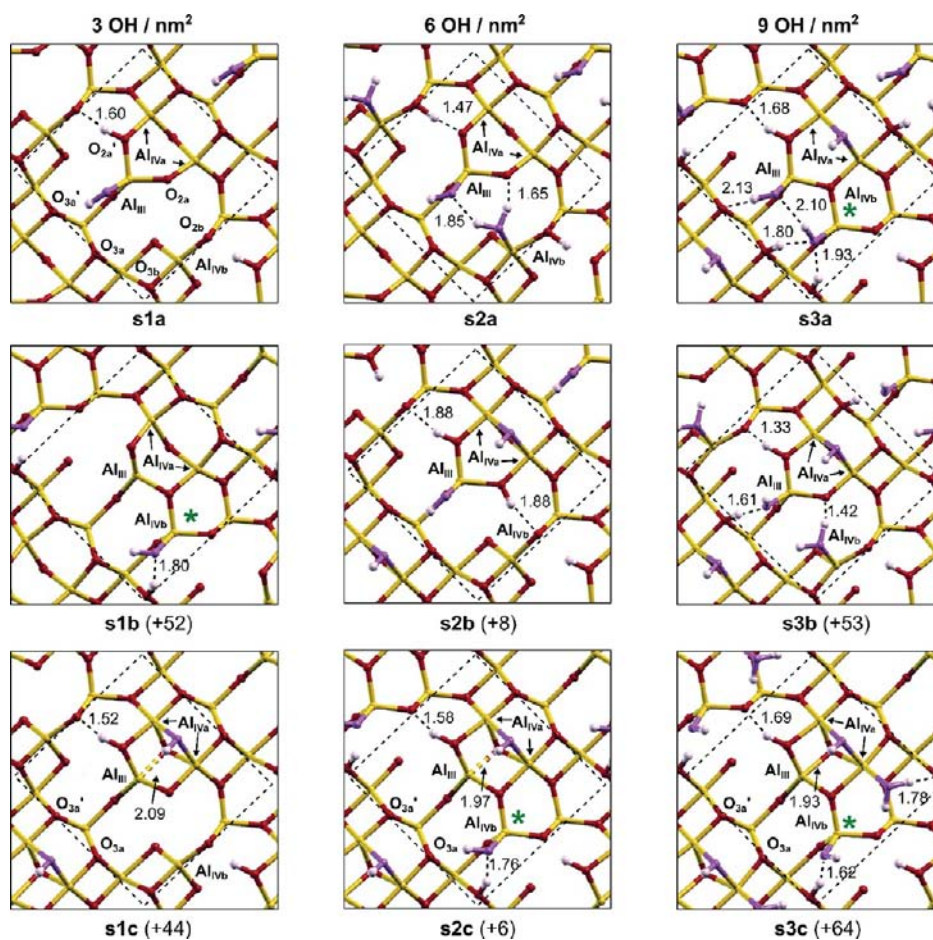


**Figure 3.** Hydroxylated terminations of alumina (110) covered by: 3 ( $s_1$ ), 6 ( $s_2$ ) and 9 ( $s_3$ ) OH  $\text{nm}^{-2}$ . The top panels correspond to the most stable configurations with hydroxylated  $\text{Al}_{\text{III}}$  sites ( $s_{ia}$ ), the middle panel to other low-energy isomers ( $s_{ib}$ ) and the bottom panels to low-energy metastable configurations with free  $\text{Al}_{\text{III}}$  sites ( $s_{ic}$ ). Only the top two layers of the periodical slab are represented. A dashed line indicates the unit cell; Al, yellow; O originating from the  $\gamma$ - $\text{Al}_2\text{O}_3$  bulk, red; O originating from  $\text{H}_2\text{O}$  dissociation, purple; H, white balls;  $\text{Al}_{\text{IV}}$  after surface reconstruction is indicated by a green star. All distances are given in Å. The stability of the surfaces relative to the corresponding  $s_{ia}$  surfaces is given in brackets ( $\text{kJ mol}^{-1}$ ).

**Table 1. Adsorption of Water Molecules on the Fully Dehydrated s0  $\gamma$ -Alumina (110) Surface forming the “sni” Surfaces<sup>a</sup>**

surface (sn) <sup>b</sup>	$n$ H <sub>2</sub> O [OH nm <sup>-2</sup> ]	adsorption site	$E_{\text{ads}}$ [kJ mol <sup>-1</sup> ] <sup>c</sup>
s1a	1 (3.0)	III, O <sub>2a</sub>	-226
s1b		IVb, O <sub>3b</sub>	-174
s1b'		IVb, O <sub>2b</sub>	-162
s1b''		IVb, O <sub>3b</sub>	-125
s1c		IVa, O <sub>2a</sub>	-182
s2a	2 (5.9)	III, IVb	-406
s2a'		III, IVb	-404
s2b		III, IVa	-398
s2b'		III, IVa	-387
s2c		IVa, IVb	-400
s2c'		IVa, IVb	-362
s3a	3 (8.9)	III, IVa, IVb	-589
s3b		III, IVa, IVb	-536
s3c		IVa, IVa, IVb	-523

<sup>a</sup>Number of surface molecules per surface unit cell (hydroxyl density, nm<sup>-2</sup>), adsorption site, and total adsorption energies  $E_{\text{ads}}$  (kJ mol<sup>-1</sup>).

<sup>b</sup>Surfaces of “sna” type correspond to the most stable situation for  $n$  water molecules adsorbed per unit cell (for a density of  $n$  OH/nm<sup>2</sup>) and associated isomers, “snb” surfaces correspond to other low-energy isomers, and “snc” surfaces conserve an Al<sub>III</sub> site. <sup>c</sup>Calculated with the bare surface s0 as reference:  $E_{\text{coads}} = E(\text{sn}) - [E(\text{s0}) + n \cdot E(\text{H}_2\text{O})]$ .

along with an OH group on O<sub>2a</sub> hydrogen bonded to O<sub>2b</sub> (s1a). The second most stable structure (s1c, 44 kJ mol<sup>-1</sup> higher in energy) has surprisingly a free Al<sub>III</sub> site, the most Lewis acidic Al atom on s0. In this case, the OH group is bridging between the two Al<sub>IVa</sub>, while the proton occupies again the most basic O<sub>2a</sub> site. This s1c termination shows a stabilizing interaction between Al<sub>III</sub> and a second-layer O atom (at 2.09 Å distance, compared to 1.76–1.82 Å for bulk tetrahedral Al–O).

Alternatively, it is also possible to occupy the Al<sub>IVb</sub> site, but the resulting structures are significantly less stable (s1b surfaces, see Figures 3 and S6), despite the fact that this site is intrinsically more Lewis acidic than Al<sub>IVa</sub>. Here, the less acidic O<sub>3b</sub> position is protonated, and the Al<sub>IVb</sub> site is reconstructed, yielding a tetrahedral Al<sub>IV</sub>–OH. This reconstruction provides a significant stabilization, the nonreconstructed isomer (s1b'', Figure S6) being less stable than s1b by 50 kJ mol<sup>-1</sup>.

**Intermediate Water Coverage (6 OH nm<sup>-2</sup>).** Based on the most stable configuration of the s1 surface, a preferred occupation of both Al<sub>III</sub> and Al<sub>IVa</sub> is expected for the s2 surface. However, this structure (s2b) is 8 kJ mol<sup>-1</sup> less stable than s2a, where Al<sub>III</sub> and Al<sub>IVb</sub> are occupied. This shows that the adsorption energy of two water molecules is not simply additive, but that it implies cooperative effects between sites. Actually, several nearly isoenergetic configurations exist with various adsorption sites. A structure keeping the reactive Al<sub>III</sub> free (s2c) is almost as stable (+ 6 kJ mol<sup>-1</sup>) as the most stable isomer where it is occupied (s2a). In view of the small energy difference, the structure with free Al<sub>III</sub> (s2c) should be considered as stable and as probable as s2a and s2b. This s2c structure is formed by adsorption of two water molecules on Al<sub>IVa</sub>, O<sub>2a</sub> and Al<sub>IVb</sub>, O<sub>3b</sub>, but the overall adsorption energy (-400 kJ mol<sup>-1</sup>) is 44 kJ mol<sup>-1</sup> higher than the sum of the individual water adsorption events (182 + 174 = 356 kJ mol<sup>-1</sup>). One can say that hydroxylation of Al<sub>IVa</sub> enhances the reactivity of the neighboring Al<sub>IVb</sub>, or vice versa, thus inducing a nonadditive/synergistic effect for water adsorption. This effect does not simply originate from the presence of specific hydrogen bonding, since these are already present in the single water adsorption structures. In this case of s2c, the reconstruction of Al<sub>IVb</sub> is again an important stabilizing effect, its absence leading to the less stable s2c' surface (by 38 kJ mol<sup>-1</sup> compared to s2c, Figure S6). As found on s1c, there is an interaction between Al<sub>III</sub> and a second-layer O atom on s2c, but it is stronger, as evidenced by the significantly shorter Al–O distance of 1.97 Å, compared to 2.09 Å on s1c.

**Table 2. Calculated Adsorption Energies and Vibrational Frequencies for N<sub>2</sub> and CO Adsorbed on the (110) and (100) Terminations of  $\gamma$ -Al<sub>2</sub>O<sub>3</sub> as a Function of Surface Hydroxylation**

N <sub>2</sub> /CO ads. site	H <sub>2</sub> O ads. site	ref. surface	$E_{\text{ads}}(\text{N}_2)$	$E_{\text{ads}}(\text{CO})$	$\Delta(\text{N}_2)$	$\Delta(\text{CO})$	$\Delta\bar{\nu}(\text{NN})^a$	$\Delta\bar{\nu}(\text{CO})^a$
			[kJ mol <sup>-1</sup> ]					
III	–	s0	-41	-74			+17	+66
	IVa	s1c	-30	-69	+11	+5	+22	+47
	IVa, IVb	s2c	-6	-38	+35	+36	+1	+43
	IVa, IVa, IVb	s3c	-7	-20	+34	+54	+2	+24
IVa/IVa'	–	s0	-8	-29			+6	+30
	III	s1a	-5	-21	+3	+8	+6	+41
	III, IVb	s2a	-4	-9	+4	+20	0	+12
IVb	–	s0	-15	-45			+5	+30
	III	s1a	-28	-60	-13	-15	+11	+60
	IVa	s1c	-19	-55	-4	-10	+6	+14
	III, IVa	s2b	-12	-38	+3	+7	+5	+29
	III, IVa	s2b'	-14	-45	+1	0	+5	+17
Va	–	s0	-11	-37			-3	+20
Vb	–	(100)	-5	-21				+4
Vc	–		-5	-21				+8
Vd	–		-5	-21				+5

<sup>a</sup>Shift of the harmonic frequency with respect to the calculated harmonic values for N<sub>2</sub> (2365 cm<sup>-1</sup>) and CO (2131 cm<sup>-1</sup>).

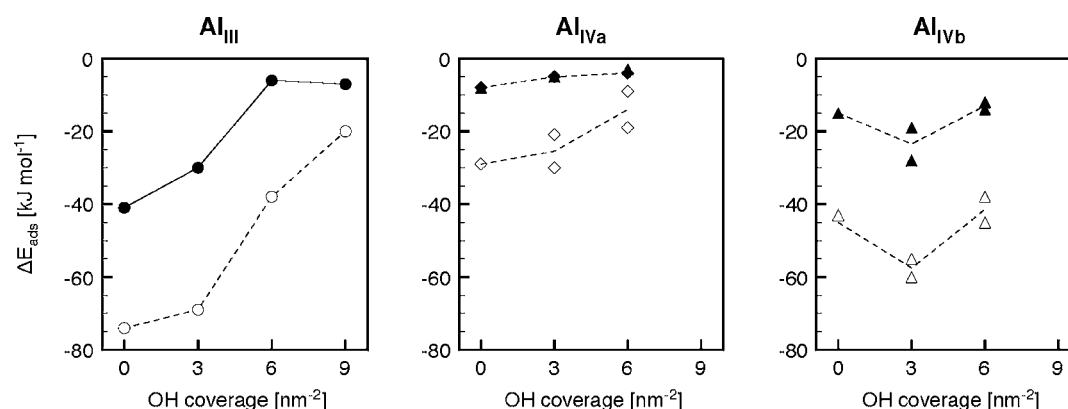


**Figure 4.** Adsorption energy of  $N_2$  (●) and CO (○) on selected Al Lewis acid sites of the  $\gamma$ - $Al_2O_3$  (110) termination as a function of OH coverage.

**High Water Coverage ( $9\text{ OH nm}^{-2}$ ).** At high water coverage, which corresponds to 3  $H_2O$  per unit cell, all Al sites are occupied in stable structures, and  $Al_{IVb}$  is reconstructed into a tetrahedral site (**s3a**). Surfaces with unreconstructed  $Al_{IVb}$ , such as **s3b**, are again much less stable. Finally, surfaces with a free  $Al_{III}$  site (e.g., **s3c**) are highly unstable ( $+66\text{ kJ mol}^{-1}$ ) and unlikely to exist even if the stabilization of  $Al_{III}$  by a second-layer O atom is more pronounced (Al–O distance of 1.93 Å), making the presence of  $Al_{III}$  on highly hydroxylated alumina improbable.

**Adsorption of Basic Probe Molecules.** The adsorption of water gave a first indication of the overall reactivity of surface sites because Lewis acidic Al and basic O surface sites are involved simultaneously in the dissociation of  $H_2O$  into  $OH^-$  and  $H^+$ . Terminations keeping the reactive  $Al_{III}$  site free can exist as low-energy metastable structures, but the  $Al_{III}$  experiences an interaction with a second-layer oxygen. This and the hydration of adjacent  $Al_{IV}$  sites might affect the reactivity of  $Al_{III}$  sites, while other sites can see their reactivity increased. Therefore, the adsorption energies of the Lewis bases  $N_2$  and CO have been used as a simple descriptor to evaluate the intrinsic Lewis acidity of Al surface sites as a function of hydration (on the various *sni* surfaces, Table 2, and Figure 4):

$$E_{\text{ads}}(\text{Mol}) = E(\text{Mol on } si) - E(si) - E(\text{Mol})$$

where Mol is either  $N_2$  or CO.

More stable adsorption is indicated by a more negative value for  $E_{\text{ads}}(\text{Mol})$ . In order to underline the influence of hydration on the adsorption, we calculated the difference  $\Delta$  between the adsorption energy on *si* and *s0* of probe molecules. Negative values for  $\Delta$  indicate cases where adsorption energy is enhanced on the partially hydrated surfaces:

$$\Delta = E_{\text{ads}}(\text{Mol}) - E_{\text{ads}}(\text{Mol})_{s0}$$

In addition, these probe molecules experience characteristic vibrational shifts upon adsorption (Table 2), which allows comparison between experimental and calculated values.

**$Al_{III}$  Site.**  $N_2$  adsorption on the  $Al_{III}$  sites leads to stable adducts (end-on coordination to Al) only in the case of **s0** and **s1c**, while no adsorption takes place on **s2c** and **s3c** (Table 2), as seen from the long Al–N distance (Table S1). The absence of adsorption of  $N_2$  for  $\theta_{OH} \geq 6\text{ nm}^{-2}$  is in good agreement with the fact that  $N_2$  does not adsorb on alumina pretreated at temperatures below  $400\text{ }^\circ\text{C}$  (Figure 1b). The adsorption energy on **s1c** is close to that on **s0**, indicating a similar Lewis acidity

of  $Al_{III}$ , while **s2c** and **s3c** surfaces display a much weaker Lewis acidity.

The CO molecule also strongly adsorbs on the  $Al_{III}$  site of **s0** and **s1c** but much more weakly (by  $36\text{ kJ mol}^{-1}$ ) on **s2c**. Note, however, that in contrast to  $N_2$ , CO adsorption takes place on the  $Al_{III}$  site of the **s2c** surface, as seen from the energy and the Al–C distance (Table S1). This is consistent with the higher basicity of CO.<sup>58</sup> Nevertheless, on the **s3c** surface, only a weak adsorption is found (long Al–C distance), demonstrating the very low acidity of  $Al_{III}$  on this surface. Qualitatively,  $N_2$  and CO give a similar picture of the Lewis acidity of  $Al_{III}$ : **s0**  $\sim$  **s1c**  $>$  **s2c**  $\gg$  **s3c**, as clearly apparent from Figure 4. The Lewis acidity steadily decreases upon hydration of the alumina surface.

**$Al_{IVa}$  Site.**  $N_2$  does not significantly adsorb on  $Al_{IVa}$ , independent of the level of hydration (**s0**–**s3**). The adsorption energy of CO is low and varies less with hydration than in the case of  $Al_{III}$ , although a destabilization of  $10$ – $20\text{ kJ mol}^{-1}$  is seen on **s2** (Figure 4). While both  $Al_{IVa}$  sites are initially equivalent on **s0**, they become slightly different on the partially hydrated surfaces.

**$Al_{IVb}$  Site.** The adsorption energy of  $N_2$  on the  $Al_{IVb}$  site of **s0** is much lower than on  $Al_{III}$ , as expected. However, on the most stable hydrated termination **s1a**, for which the neighboring  $Al_{III}$  site is hydroxylated, the adsorption on  $Al_{IVb}$  becomes surprisingly stronger than on the same site on **s0** (by  $13\text{ kJ mol}^{-1}$ ), making it close to that on  $Al_{III}$  of **s1c**. Such a stabilizing but weaker ( $4\text{ kJ mol}^{-1}$ ) effect is also found on **s1c**. An enhancement of Lewis acidity of an Al surface site of alumina from water adsorption on a neighboring Al site is unexpected and has not been reported before to our knowledge. Note also that the Al–N distance is 2.22 Å on **s1a**, hence shorter compared to that on **s0** (2.31 Å, see Table S1). This suggests that hydroxylation modifies the Lewis acidity of neighboring Al sites. Note that a similar albeit weaker enhancement is also found on the **s1c** surface, i.e., when  $Al_{IVa}$  is occupied. At higher water coverage (**s2b** and **s2b'**,  $6\text{ OH nm}^{-2}$ ) a weaker adsorption is found, comparable to that on **s0**. Adsorption of the CO molecule gives a similar picture. On **s0**, CO adsorption on  $Al_{IVb}$  is significantly weaker than on  $Al_{III}$ , but CO on  $Al_{IVb}$  is stabilized by  $15\text{ kJ mol}^{-1}$  on **s1a**. As found for  $N_2$ , we find a stabilizing, albeit weaker ( $10\text{ kJ mol}^{-1}$ ) effect on **s1c**. Again the overall adsorption energies of CO on  $Al_{IVb}$  are higher than those of  $N_2$ , but the same trend regarding Lewis acidity is found: **s1a**  $>$  **s1c**  $>$  **s0**  $\sim$  **s2b'**  $>$  **s2b**. Hence for that site, a nonlinear influence of hydration is seen, with an optimum on **s1** ( $3\text{ OH nm}^{-2}$ ) (see Figure 4).

**Table 3.** Comparison of Experimental IR bands for the Adsorption of CO on  $\gamma$ - and  $\delta$ -Al<sub>2</sub>O<sub>3</sub> (Gribov et al., ref 42) with Calculated Values<sup>a</sup>

$\tilde{\nu}(\text{CO})$ ( $\Delta\tilde{\nu}(\text{CO})_{\text{exp}}$ )	$\Delta\tilde{\nu}(\text{CO})_{\text{calc}}$	lit. assignment	our work	surface	$\Theta(\text{OH})$
[cm <sup>-1</sup> ]					[nm <sup>-2</sup> ]
2200–2190 (+57/+47)	+66	III	III	s0	0
	+47		III	s1c	3
	+43		III	s2c	6
	+60		IVb	s1a	3
2184–2173 (+41/+30)	+47	IV	III	s1c	3
	+43			s2c	6
	+30	IVa	s0	0	
	+25/+41		s1a	3	
	+12/+23		s2a	6	
	+30	IVb	s0	0	
2153–2148 (+10/+5)	+4/+5/+8/+20	V	Va–Vd (100)	s0	0

<sup>a</sup>Weak bands at 2230 and 2230 attributed to defects sites (step, corners) are not considered.

*Al<sub>V</sub> on (100).* As mentioned before, the (100) termination is not hydrated in the temperature range investigated here. N<sub>2</sub> is only very weakly stabilized on Al<sub>Va</sub> (–11 kJ mol<sup>-1</sup>) while on the Al<sub>Vb</sub>, Al<sub>Vc</sub> and Al<sub>Vd</sub> sites no adsorption takes place. For CO, the stabilization on Al<sub>Va</sub> is more significant (–37 kJ mol<sup>-1</sup>) and higher than on the other sites of this termination. Overall the Lewis acidity can be ranked as follows: Al<sub>Va</sub> > Al<sub>Vb</sub> = Al<sub>Vc</sub> = Al<sub>Vd</sub>.

*Calculated Vibrational Shifts and Adsorption Enthalpies Compared to Experiment.* On  $\gamma$ -alumina treated above 400 °C, three to five bands resulting from CO adsorption can be distinguished, but their positions, widths, and intensities are variable. This depends on the CO coverage (due to adsorbate–adsorbate interactions), the alumina phase, the pretreatment temperature of the sample, and the temperature of CO adsorption. The most recent low-temperature CO adsorption experiments on  $\gamma$ - and  $\delta$ -Al<sub>2</sub>O<sub>3</sub> pretreated at 750 °C reveal three major bands at 2200–2190, 2184–2173, and 2153–2148 cm<sup>-1</sup>, which correspond to a shift of the CO vibration to higher frequency by 47–57, 30–41, and 5–10 cm<sup>-1</sup>, respectively.<sup>42</sup> These bands were assigned to CO adsorbed on three-, four-, and five-coordinate Al atoms on extended surfaces (III, IV, and V in Table 3). Note also that very weak bands at 2215 (+72) and 2230 (+87) cm<sup>-1</sup> have been reported and assigned to Al sites located on edges, steps, and corners of Al<sub>2</sub>O<sub>3</sub> particles.<sup>42,46</sup> Moreover, the initial enthalpy of adsorption of CO, i.e., at zero coverage (on the most Lewis acidic sites), measured by microcalorimetry is ca. 60 kJ mol<sup>-1</sup> when pretreated at 500 °C,<sup>59</sup> while it is only 40 kJ mol<sup>-1</sup> for a pretreatment temperature of 400 °C. This shows that high pretreatment temperatures are necessary to form the stronger adsorption sites. This high initial enthalpy (60 kJ mol<sup>-1</sup>) associated with high-frequency shift of 47–57 cm<sup>-1</sup> is in good agreement with not only the values calculated for the most Lewis acidic Al<sub>III</sub> sites on s0/s1c but also with these associated with the Al<sub>IVb</sub> site on s1a. Thus, the band at 2200–2190 cm<sup>-1</sup> can be attributed to both three- and four-coordinate Al sites, clearly showing that unambiguous assignment of the multiple CO bands based on the coordination number of Al is dangerous. Therefore, while CO is historically the most used probe for Lewis acid sites, it cannot be considered as a selective probe.

In contrast, N<sub>2</sub> acts as a very selective probe toward the most Lewis acidic sites. The N–N vibration is shifted by +17 and

+22 cm<sup>-1</sup> on the s0 and s1c surfaces, respectively, which compares favorably with the experimental shift of +25 cm<sup>-1</sup>,<sup>39</sup> note also, as in the case of CO, the rather strong blue shift on Al<sub>IVb</sub> of s1a (+11 cm<sup>-1</sup>). All other sites do not show any appreciable shift of the N–N vibration, in contrast to CO, which also adsorbs on Al<sub>IVa</sub> and Al<sub>V</sub> sites (the latter being only present on the (100) termination).

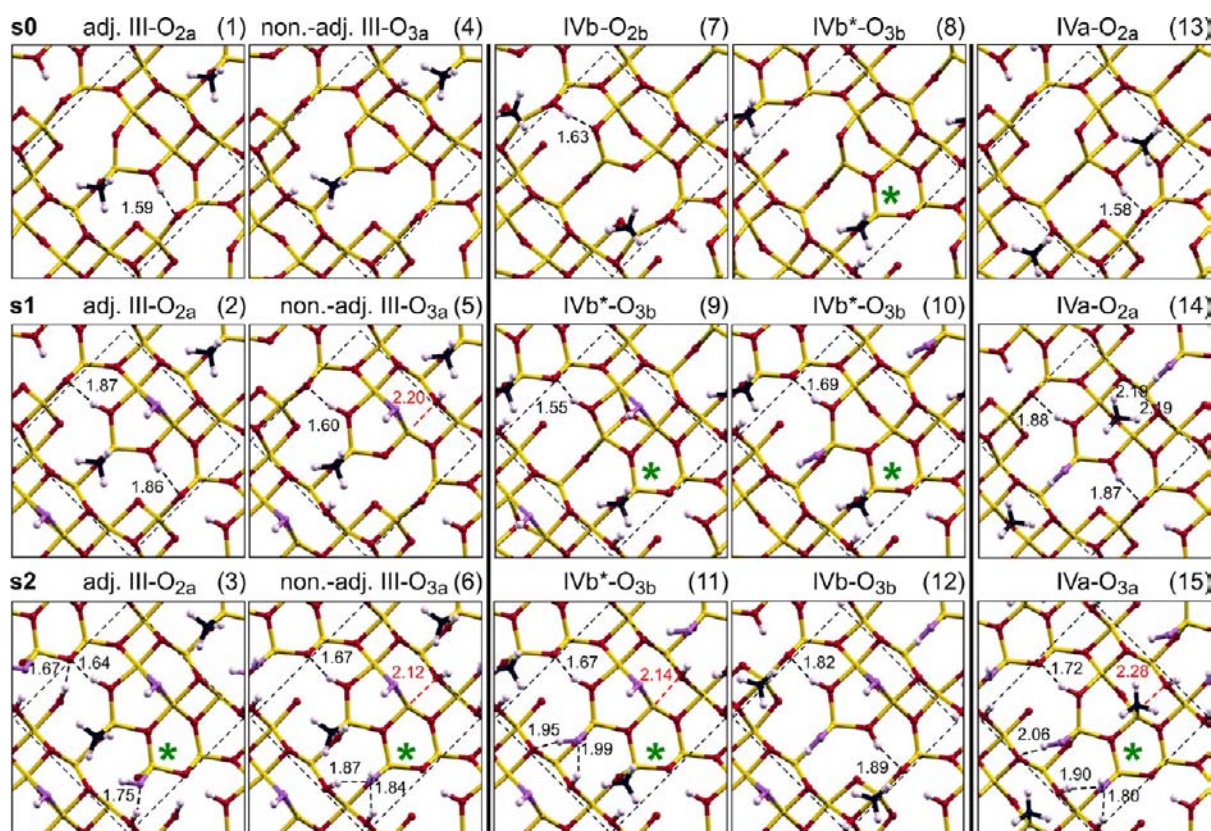
**Methane Dissociation: Reaction on Al<sub>2</sub>O Sites of the Fully Dehydroxylated Surface (s0).** The case of methane, already presented in part for the Al<sub>III</sub> site in ref 41, will be described for comparison and complemented by including other Al sites. The dissociation reaction of CH<sub>4</sub> on Al<sub>2</sub>O sites leads to the formation of Al–methyl (Al–CH<sub>3</sub>) and hydroxyl (O–H) species as the only stable products. The formation of Al–hydride (Al–H) and methoxy species (O–CH<sub>3</sub>) is always highly endoenergetic (+62 to +131 kJ mol<sup>-1</sup>) and in all cases associated with a prohibitively high TS energy, e.g., +282 kJ mol<sup>-1</sup> on Al<sub>III</sub> (Table S2).

The dissociation can occur on adjacent Al<sub>2</sub>O sites, i.e., Al is directly bonded to O, or nonadjacent sites, where the O is not directly bonded but faces the Al atom (Al–O distance of 4.10 Å, see Table 4). On s0, the reaction is most favorable on sites composed of the tricoordinate Al<sub>III</sub> and an adjacent dicoordinate O<sub>2a</sub> atom ( $E_{\text{ads}} = -84$  kJ mol<sup>-1</sup>, Table 4, structure 1), while it is endoenergetic when the proton is attached to a nonadjacent tricoordinate O<sub>3a</sub> atom ( $E_{\text{ads}} = +18$  kJ mol<sup>-1</sup>, 4). The process is still slightly exoenergetic on Al<sub>IVb</sub> ( $E_{\text{ads}} = -15$  kJ mol<sup>-1</sup>, 7), but it becomes endoenergetic on Al<sub>IVa</sub> ( $E_{\text{ads}} = +24$  kJ mol<sup>-1</sup>, 13). We also find a relatively favorable dissociation followed by surface reconstruction on the (Al<sub>IVb</sub>, O<sub>3b</sub>) site ( $E_{\text{ads}} = -17$  kJ mol<sup>-1</sup>, 8). Here, instead of becoming five-coordinate, the initial Al<sub>IVb</sub> site ends up in a tetrahedral configuration, as already seen above in the case of water adsorption. Finally, dissociative adsorption on the (100) surface is highly unfavorable (+76 kJ mol<sup>-1</sup>), again showing the low reactivity of this termination.

The reaction pathways for the dissociation of CH<sub>4</sub> on s0 are characterized by weakly bound precursor state (PS) and TS energies ranging in energy from +64 to +116 kJ mol<sup>-1</sup> (Table 4). A PS associated with a significant stabilization of CH<sub>4</sub> (–24 kJ mol<sup>-1</sup>) was only found on the most Lewis acidic Al<sub>III</sub> site. The geometry of the PS is characterized by a H–C–H moiety of methane coordinated on Al ( $\sigma$ -complex), as indicated by two

**Table 4. Structure of the Product, Reaction Energy ( $E_{\text{diss}}$ ), Influence of Hydration ( $\Delta$ ), Energy of the Precursor State ( $E_{\text{preads}}$ ), and TS ( $E_{\text{TS}}$ ) for the Dissociation of  $\text{CH}_4$  on (Al,O) Sites of the  $\gamma\text{-Al}_2\text{O}_3$  (110) Termination<sup>a</sup>**

	CH <sub>4</sub> ads. site	H <sub>2</sub> O ads. site	ref surface	$E_{\text{diss}}(\text{CH}_4)$	$\Delta$	$E_{\text{preads}}(\text{CH}_4)$	$E_{\text{TS}}(\text{CH}_4)$	$\delta^{13}\text{C}$
				[kJ mol <sup>-1</sup> ]				
1		–	s0	–84	–	–24	+64	–13
2	III <sub>l</sub> O <sub>2a</sub> /O <sub>2a</sub> '	IVa	s1c	–65	+19	–12	+74	–10
3		IVa, IVb	s2c	–10	+74	–6	+116	–6
4		–	s0	+18	–	–24	+86	–11
5	III <sub>l</sub> O <sub>3a</sub> /O <sub>3a</sub> '	IVa	s1c	–26	–44	–12	+45	–9
6		IVa, IVb	s2c	–22	–40	–6	+103	–5
7	IVb <sub>l</sub> O <sub>2b</sub>	–	s0	–15	–	–7	+79	–11
8		–	s0	–17	–	–7	+98	–13
9		IVa	s1c	–53	–36	–	+72	–11
10	IVb <sub>l</sub> O <sub>3b</sub>	III	s1a	–6	+11	–11	+83	–10
11		III, IVa	s2b'	–27	–10	–	+90	–6
12		III, IVa	s2b	+46	+63	–	–	–8
13		–	s0	+24	–	–4	+116	–6
14	IVa <sub>l</sub> O <sub>2a/3a</sub>	III	s1a	+45	+21	–	–	4
15		III, IVb	s2a'	+15	–9	–	–	–4
–	V <sub>l</sub> O <sub>3</sub>	–	s0 (100)	+76	–	–	–	4



<sup>a</sup>Only the top two layers of the periodical slab are represented. A dashed line indicates the surface unit cell; Al, yellow; O originating from the  $\gamma\text{-Al}_2\text{O}_3$  bulk, red; O originating from  $\text{H}_2\text{O}$  dissociation, purple; H, white balls; C, black balls; and  $\text{Al}_{\text{IVb}}$  after surface reconstruction is indicated by a green star. All distances are given in Å.

roughly equal Al–H distances (2.1–2.2 Å) (Figure S7). This is accompanied by a slight weakening of the C–H bonds of methane coordinated to Al. Note also, that the corresponding H–C–H angle (117.9°) deviates from that in the free molecule (109.4°).

The TSs are structurally very similar on all sites with four atoms sharing the same plane, wide C–H–O and acute O–Al–C angles (Table S3 and Figure S8). The C–H bond of methane is elongated by ca. 30% with respect to its equilibrium distance

in the gas phase (1.10 Å), and the Al–C bond length is closer to its final value than the OH bond. On the nonadjacent  $\text{Al}_{\text{III}}\text{O}_{3a}$  site the C–H and Al–C bonds are slightly more elongated than on the adjacent  $\text{Al}_{\text{III}}\text{O}$  sites and the C–H–O<sub>2a</sub> angle is almost linear (171°), which is optimal for a 3-center, 4-electron TS. Despite the endoenergetic reaction, the TS energy on the nonadjacent  $\text{Al}_{\text{III}}\text{O}_{3a}$  is only 12 kJ mol<sup>-1</sup> higher than on the adjacent  $\text{Al}_{\text{III}}\text{O}_{2a}$  site.

**Methane Dissociation: Reaction on Al<sub>IV</sub>O Sites of the Partially Hydrated Surface (si).** The influence of partial hydration of alumina on CH<sub>4</sub> dissociation was studied by probing the reactivity of remaining unsaturated Al–O sites on **s1** and **s2** models (Table 4), including the metastable terminations considered as “defect” sites. In view of the high adsorption energy of H<sub>2</sub>O, the reaction of methane on alumina will never involve desorption of H<sub>2</sub>O prior to C–H activation. We will therefore look at the adsorption energy of CH<sub>4</sub> on a corresponding hydrated **si** surface in order to investigate the influence of hydration on the reaction energy:

$$E_{\text{diss}}(\text{CH}_4) = E(\text{si} + \text{CH}_4) - E(\text{si}) - E(\text{CH}_4)$$

where **si** + CH<sub>4</sub> is the **si** surface with the dissociated CH<sub>4</sub> molecule. The effect of hydration on the stability of Al–CH<sub>3</sub> becomes again most easily apparent by defining the energy  $\Delta$ , which is the difference between the dissociation energies of CH<sub>4</sub> on **si** and **s0**:

$$\Delta = E_{\text{diss}}(\text{CH}_4)_{\text{si}} - E_{\text{diss}}(\text{CH}_4)_{\text{s0}}$$

The sign and the value of  $\Delta$  in Table 3 directly show the influence of hydration on the reaction of CH<sub>4</sub> on a specific Al<sub>IV</sub>O site, with a negative  $\Delta$  value describing a reaction favored by hydration. The same approach will be applied later to the dissociation of H<sub>2</sub>.

**Low Water Coverage (3 OH nm<sup>-2</sup>).** For a hydroxyl density of 3 OH nm<sup>-2</sup> (one H<sub>2</sub>O per unit cell), the dissociation of CH<sub>4</sub> is most favorable when it occurs on the metastable **s1c** termination, either on the adjacent Al<sub>III</sub>O<sub>2a</sub> site (structure 2 in Table 4,  $E_{\text{diss}}(\text{CH}_4) = -65$  kJ mol<sup>-1</sup>) or on Al<sub>IVb</sub>O<sub>3b</sub>, (**9**,  $E_{\text{diss}}(\text{CH}_4) = -53$  kJ mol<sup>-1</sup>). In the latter case it is associated with reconstruction of Al<sub>IVb</sub> into a tetrahedral site. Note that hydroxylation on Al<sub>IVa</sub> disfavors the dissociation on the Al<sub>III</sub>O<sub>2a</sub> site ( $\Delta = +19$ ), whereas it strongly favors that on the Al<sub>IVb</sub>O<sub>3b</sub> site ( $\Delta = -36$ ). A similar synergy between Al<sub>IVa</sub>O<sub>2a</sub> and Al<sub>IVb</sub>O<sub>3b</sub> was already underlined above on **s1c** for dissociative adsorption of water ( $\Delta = -44$ ), but for the pure probes of acidity N<sub>2</sub> and CO, the influence of Al<sub>IVa</sub> hydroxylation on Al<sub>IVb</sub> is weaker ( $\Delta = -4$  or  $-10$ , respectively, see Table 2). For the nonadjacent Al<sub>III</sub>O<sub>3a</sub> site, a similar strong favorable synergy effect ( $\Delta = -44$ ) is found on **s1c** (**5**), where the reaction energy goes from +18 on **s0** (**4**) to  $-26$  kJ mol<sup>-1</sup> even if the Lewis acidity of Al<sub>III</sub> is decreased on **s1c**. These contrasts between the influence of hydroxylation on CH<sub>4</sub> and CO/N<sub>2</sub> reactivity, and the strong difference between Al<sub>III</sub>O<sub>2a</sub> and Al<sub>III</sub>O<sub>3a</sub> sites upon hydroxylation of Al<sub>IVa</sub> suggests that hydroxylation of a neighboring Al not only affects the Al Lewis acidity but also the basicity of oxygen atoms. On **s1a**, where Al<sub>III</sub> is occupied by an OH group, the dissociation of CH<sub>4</sub> on the remaining Al<sub>IVb</sub> and Al<sub>IVa</sub> sites is not favorable (structures **10** and **14**, positive  $\Delta$ ). Although it is again followed by reconstruction, the dissociation on Al<sub>IVb</sub>O<sub>3b</sub> is much less favorable than on **s1c**, which shows that the position of the OH group (on Al<sub>III</sub> or Al<sub>IVa</sub>) has a significant influence on the reaction energy of CH<sub>4</sub> on a given Al–O pair.

**Intermediate Water Coverage (6 OH nm<sup>-2</sup>).** For an alumina surface covered with two H<sub>2</sub>O molecules per unit cell (6 OH nm<sup>-2</sup>), the reaction is most favorable on the nonadjacent Al<sub>III</sub>O<sub>3a</sub> site of **s2c** (**6**,  $E_{\text{diss}} = -22$  kJ mol<sup>-1</sup>,  $\Delta = -40$ ). This contrasts with the strong decrease of reaction energy on the Al<sub>III</sub>O<sub>2a</sub> site ( $\Delta = +74$ ) and points again to the strong influence of hydroxylation on the basicity of surface O atoms. Methane dissociation is also favored on the Al<sub>IVb</sub>O<sub>3b</sub> site

of **s2b'**, i.e., when the surface can be reconstructed, forming a tetrahedral Al<sub>IVb</sub> site (**11**,  $E_{\text{diss}} = -27$  kJ mol<sup>-1</sup>,  $\Delta = -10$ ). The **s2b'** surface (see Figure S6) is an isomer of the **s2b** surface (19 kJ mol<sup>-1</sup> less stable than **s2a**) where the proton on O<sub>2a</sub> has formally migrated to O<sub>3a</sub>, thus allowing reconstruction of Al<sub>IVb</sub>. Note that adsorption on **s2b** (**12**), where this reconstruction is not possible, is highly unfavorable. The reaction is hence again favored by hydration, however it remains much less exoenergetic than on the Al<sub>III</sub>O<sub>2a</sub> site of **s1** or **s0**, which indicates that higher OH coverage (6 OH nm<sup>-2</sup>) is globally detrimental to the dissociation of CH<sub>4</sub> on alumina. Concerning the Al<sub>IVb</sub>O<sub>3b</sub> site, we find that occupation of the neighboring Al<sub>III</sub> by an OH group disfavors the dissociation of CH<sub>4</sub>, when comparing **9** and **11**. This effect is similar to what was found on **s1**.

**Calculated <sup>13</sup>C NMR Chemical Shifts for Al–CH<sub>3</sub> Species.** For comparison with experimental <sup>13</sup>C NMR data (a single peak at  $-22$  ppm),<sup>40</sup> we calculated the chemical shift for the carbon atom of the Al–CH<sub>3</sub> group (Table 4). The values fall within a small range, which does not allow a clear distinction between sites. Tetrahedral species formed on Al<sub>III</sub> or on Al<sub>IVb</sub> followed by reconstruction are closest (by ca. 10 ppm) to experiment, while the endoenergetic methyl species formed on the Al<sub>IVa</sub> and Al<sub>V</sub> sites are the least compatible. Note, that the calculated chemical shift for methoxy species is around 60 ppm (Table S2), therefore their presence can be safely excluded. Combining the calculated chemical shifts and reaction energies, the most probable site of C–H activation is therefore Al<sub>III</sub>.

**Methane Dissociation: Effect of Hydration on the Reaction Pathways.** The reaction pathways have been investigated for the most favorable cases, i.e., for dissociation of CH<sub>4</sub> on Al<sub>III</sub>O<sub>2a</sub>/O<sub>3a</sub> and Al<sub>IVb</sub>O<sub>3b</sub> sites of the hydrated alumina surfaces **s1c**, **s2c**, and **s2b'** and compared to **s0** (Table 4). The corresponding TSs are represented in Figure 5. Detailed structural parameters are summarized in the Table S3.

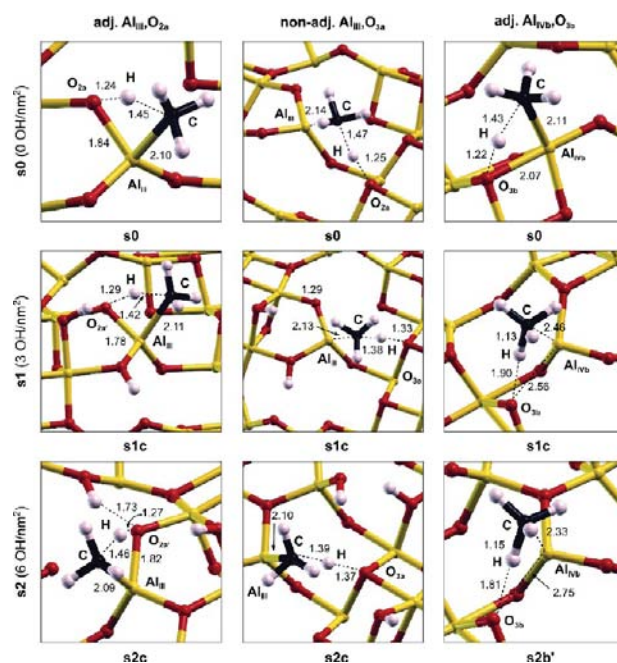
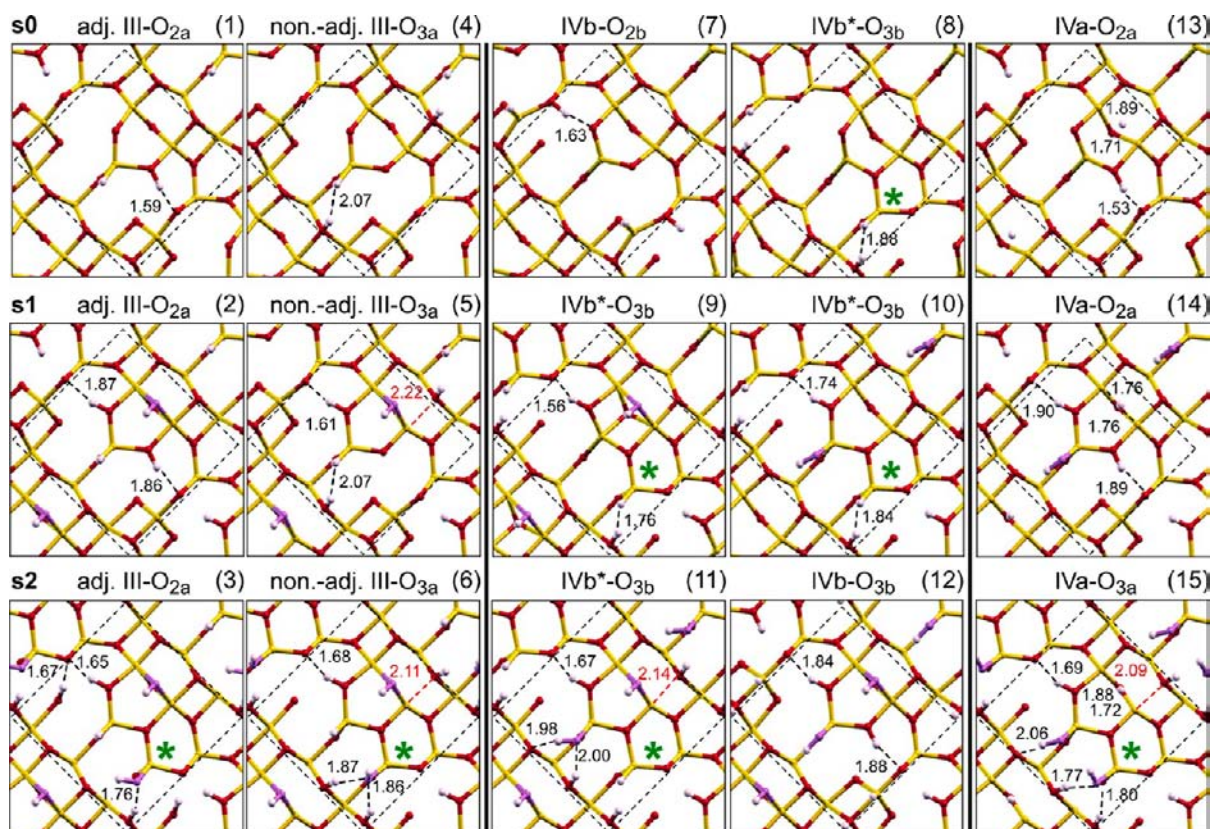


**Figure 5.** Geometry of the TS for the dissociation of CH<sub>4</sub> on three sites (adjacent Al<sub>III</sub>O<sub>2a</sub>, nonadjacent Al<sub>III</sub>O<sub>3a</sub>, and Al<sub>IVb</sub>O<sub>3b</sub>) for three OH coverages (0, 3, and 6 OH/nm<sup>2</sup>).

**Table 5. Structure of the Product, Reaction Energy ( $E_{\text{diss}}$ ), Influence of Hydration ( $\Delta$ ), Energy of the Precursor State ( $E_{\text{preads}}$ ), and TS ( $E_{\text{TS}}$ ) for the Dissociation of  $\text{H}_2$  on (Al,O) Sites of the  $\gamma\text{-Al}_2\text{O}_3$  (110) Termination<sup>a</sup>**

	$\text{H}_2$ ads. site	$\text{H}_2\text{O}$ ads. site	ref surface	$E_{\text{diss}}(\text{H}_2)$	$\Delta$	$E_{\text{preads}}(\text{H}_2)$	$E_{\text{TS}}(\text{H}_2)$	$\bar{\nu}(\text{Al-H})$
				[kJ mol <sup>-1</sup> ]				
1		–	s0	–114	–	–23	+34	1925
2	III, O <sub>2a</sub> /O <sub>2a</sub> '	IVa	s1c	–93	+21	–15	+43	1946
3		IVa, IVb	s2c	–42	71	–5	+85	1922
4		–	s0	–18	–	–23	+27	1768
5	III, O <sub>3a</sub> /O <sub>3a</sub> '	IVa	s1c	–66	–48	–15	–4	1821
6		IVa IVb	s2c	–59	–41	–5	+55	1900
7	IVb, O <sub>2b</sub>	–	s0	–44	–	–11	+43	1924
8		–	s0	–54	–	–11	+61	1864
9		IVa	s1c	–93	–39	–	+57	1845
10	IVb, O <sub>3b</sub>	III	s1a	–40	+14	–19	+55	1887
11		III, IVa	s2b'	–74	–20	–	+75	1839
12		III, IVa	s2b	+10	+61	–	–	1813
13		–	s0	–40	–	–4	+76	1460/1053
14	IVa, O <sub>2a</sub> /3a	III	s1a	–31	+14	–	–	1356/1335
15		III, IVb	s2a'	–41	+1	–	–	1456/1251
–	V, O <sub>3</sub>	–	s0 (100)	+25	–	–	–	1895



<sup>a</sup>Only the top two layers of the periodical slab are represented. A dashed line indicates the surface unit cell; Al, yellow; O originating from the  $\gamma\text{-Al}_2\text{O}_3$  bulk, red; O originating from  $\text{H}_2\text{O}$  dissociation, purple; H, white balls; and Al<sub>IVb</sub> after surface reconstruction is indicated by a star. All distances are given in Å.

**Preadorption States.** The interaction of  $\text{CH}_4$  with Al<sub>III</sub> leads to stable Lewis acid–base complexes only on s0 and on s1c (adsorption energy reduced by 10 kJ mol<sup>-1</sup> compared to s0). On s2c no significant adsorption takes place, as already found for  $\text{N}_2$ . Overall, the more the surface is hydrated, the less the  $\text{CH}_4$  complex is stabilized, in good correlation with the decrease of Al Lewis acidity.

**TSs on the Adjacent Al<sub>III</sub>O<sub>2a</sub> Site.** The energy of the TS for the dissociation of  $\text{CH}_4$  on adjacent Al<sub>III</sub>O<sub>2a</sub> sites increases with

water coverage, going from +64 (s0) to +74 (s1c) and +116 kJ mol<sup>-1</sup> (s2c), while the reaction becomes less exoenergetic. Yet, the TS geometries are nearly identical with the typical coplanar arrangement of C, O<sub>2a</sub>, Al<sub>III</sub>, and H and the wide C–H–O and acute H–Al–O angles (Table S3); the TS on s1c being slightly earlier than on s0.

**TSs on the Nonadjacent Al<sub>III</sub>O<sub>3a</sub> Site.** Surprisingly, the TS energies for C–H bond activation on nonadjacent Al<sub>III</sub>O<sub>3a</sub> sites follow an unexpected nonregular behavior with increasing water

coverage, first decreasing from +86 (**s0**) to +45 (**s1c**) and then increasing to +103 kJ mol<sup>-1</sup> (**s2c**). Noteworthy, the TS energy is lower in the presence of water on a neighboring Al<sub>IVa</sub> (**s1c**), which follows the behavior of the reaction energy discussed above and is, again, unexpected since the Lewis acidity on **s1c** is slightly lower than on **s0**, as shown by N<sub>2</sub> and CO adsorption.

In contrast to the reaction on adjacent Al<sub>I</sub>O sites, the TS geometry is affected by hydration. While the Al–C distance is similar, the C–H distance is significantly shortened on hydrated surfaces (1.47, 1.38, and 1.39 Å on **s0**, **s1c**, and **s2c**, respectively, see also Table S3), and the H–O<sub>3a</sub> distance is increased (1.25, 1.33, and 1.37 Å). This is an evidence for earlier TS's on partially hydrated surfaces, consistent with the more exoenergetic reaction on the hydrated surfaces.

**TSs on the Al<sub>IVb</sub>O<sub>3b</sub> Site.** The TS for CH<sub>4</sub> dissociation on the Al<sub>IVb</sub>O<sub>3b</sub> site leads to final geometries with a restructured Al<sub>IVb</sub> site. The TS energy is decreased when going from **s0** to **s1c** but increased on **s2b'**. The TS geometry is also affected by hydration (Figure 5 and Table S3): On **s0** the TS corresponds to the dissociation of the C–H bond on the Al<sub>IVb</sub>O<sub>3b</sub> site and is followed by a barrier-less surface reconstruction. In contrast, on **s1c** and **s2c**, for the most favorable pathway, the TS is associated to the reconstruction of the Al<sub>IVb</sub> site, the CH<sub>4</sub> molecule being almost not affected. The Al<sub>IVb</sub>–O<sub>2a</sub> bond of the new tetrahedral Al<sub>IVb</sub> is already formed (on **s1c**: 1.86 Å compared to 1.83 Å in the final product, structure 3 in Table 4) and Al<sub>IVb</sub>–O<sub>3b</sub> is broken (2.56 Å compared to 3.18 Å in the final product). In the TS, the originally tetracoordinate Al atom becomes tricoordinate, and the originally tricoordinate O atom becomes dicoordinate. This is reminiscent of what was found for the nonadjacent Al<sub>III</sub>O<sub>3a</sub> case. In the end, the reactive entities are the same: a highly reactive Lewis acid–base pair consisting of tricoordinate Al<sub>III</sub> and dicoordinate O<sub>2</sub>, but in the case of Al<sub>IVb</sub>O<sub>3b</sub>, this has to be reached through reconstruction of the surface. In this TS the C–H bond is only slightly elongated, and CH<sub>4</sub> is coordinated to the newly formed “Al<sub>III</sub>” center. In the following part of the pathway the CH<sub>4</sub> molecule is dissociated with no further barrier on this distorted reactive alumina surface site.

The different mechanisms are supported by the vibrational modes corresponding to the TS: On **s1c** and **s2c** the imaginary frequency is very low (99 and 65 cm<sup>-1</sup>, respectively), and it mainly corresponds to lattice vibrations centered on Al<sub>IVb</sub> and O<sub>3b</sub>, while on **s0** the imaginary frequency is 1092 cm<sup>-1</sup> and clearly corresponds to the C–H bond being disrupted.

Note, that on **s1c** and **s2c**, a second pathway was found, similar to that on **s0**, with a TS associated to the C–H bond breaking on the nonreconstructed surface, followed by a nonactivated reconstruction process. This pathway is however less favorable with a barrier ca. 20 kJ mol<sup>-1</sup> higher. Hydration indeed affects the C–H activation and facilitates the reconstruction process, hence promoting the switch from one pathway to the other.

**Hydrogen Dissociation.** The dissociative adsorption of H<sub>2</sub> on the  $\gamma$ -Al<sub>2</sub>O<sub>3</sub> surface (Table 5) shows strong similarities compared with methane, hence we will only discuss the most salient features and compare them to what was found for CH<sub>4</sub>. The dissociation leads to Al–H and Al–OH species, and the final structures are almost identical to those obtained by reaction with CH<sub>4</sub>, replacing Al–CH<sub>3</sub> by Al–H. The main difference is that the dissociation of H<sub>2</sub> is always more exoenergetic, typically by ca. 30 kJ mol<sup>-1</sup>. However on the Al<sub>IVa</sub>O<sub>2a</sub> site, it is even more exoenergetic by 60 kJ mol<sup>-1</sup>

because a relatively stable bridging hydride is formed in place of a terminal methyl. Note that despite the more exoenergetic reaction of H<sub>2</sub>, dissociation on Al<sub>V</sub> sites of the (100) terminations remains endoenergetic, as found for CH<sub>4</sub> ( $E_{\text{diss}} > +25$  kJ mol<sup>-1</sup>), showing that this surface is not reactive.

At the same time the associated TS are lower in energy, typically by ca. 30 kJ mol<sup>-1</sup> compared to CH<sub>4</sub>, except on the nonadjacent Al<sub>III</sub>O<sub>3a</sub> sites where the barrier is lowered by ca. 50 kJ mol<sup>-1</sup>. The pathways for H<sub>2</sub> dissociation strongly parallel those found for CH<sub>4</sub>. Note that the preadsorption state on Al<sub>III</sub> shows a clear interaction between the  $\sigma$  density of H<sub>2</sub> and the Al center. This is accompanied by a stretching of the H–H bond because of electron donation to Al (Figure S7). The TSs are associated with an open H–H–O arrangement, which is almost linear on the nonadjacent Al<sub>III</sub>O<sub>3a</sub> site and with a dihedral angle Al–H–H–O close to zero (Figures S8 and S9 and Table S4). TSs associated with the reconstruction of the Al<sub>IVb</sub> site (longer Al–O distances) and with negligible H–H activation are also found on the Al<sub>IVb</sub>O<sub>3b</sub> site of hydrated surfaces.

**Influence of Water Coverage.** The effect of hydration on the reaction energy is the same as for CH<sub>4</sub> ( $\Delta$  values differ by less than 5 kJ mol<sup>-1</sup>, see Tables 3 and 4). Because of the more exothermic reaction, the dissociation of H<sub>2</sub> is favorable from a thermodynamic point of view on all unsaturated sites of the (110) surface (Al<sub>III</sub>, Al<sub>IVa</sub>, and Al<sub>IVb</sub>) at low to intermediate water coverage (3–6 OH nm<sup>-2</sup>). The TS energy for the H–H bond activation on adjacent Al<sub>III</sub>O<sub>2a</sub> sites (Table 5) increases with water coverage, going from 34 (**s0**) to 43 (**s1c**) to 85 kJ mol<sup>-1</sup> (**s2c**). In contrast, on nonadjacent Al<sub>III</sub>O<sub>3a</sub> sites it first decreases with the water coverage from +27 (**s0**) to –4 (**s1c**, here the barrier from the precursor state is only 11 kJ mol<sup>-1</sup>) and then increases again to +55 kJ mol<sup>-1</sup> (**s2c**). Hydration has a strong impact on the TS geometry for that site (Figure S9 and Table S6), with a TS even more reactant-like than for CH<sub>4</sub> (longer Al–O and O–H distances and a less elongated H–H bond, compared to C–H).

The TS energy for H<sub>2</sub> dissociation on the Al<sub>IVb</sub>O<sub>3b</sub> site, which leads to final structures with a restructured Al<sub>IVb</sub> site, shows smaller variations with water coverage than in the case of CH<sub>4</sub>, going from +61 (**s0**) to +57 (**s1c**) and +75 kJ mol<sup>-1</sup> (**s2b'**). The TS geometry has again a different nature on the hydrated and nonhydrated surfaces (Figure S9 and Table S4). While on **s0** the TS consists in the dissociation of H<sub>2</sub> on the Al<sub>IVb</sub>O<sub>3b</sub> site, followed by surface reconstruction, the favored TSs on **s1c** and **s2b'** are associated with the reconstruction of the Al<sub>IVb</sub> site, followed by a barrierless H<sub>2</sub> dissociation. These different mechanisms are confirmed by imaginary frequencies of 216 and 346 cm<sup>-1</sup> on **s1** and **s2c** (lattice vibrations centered on Al<sub>IVb</sub> and O<sub>3b</sub>), compared to 1004 cm<sup>-1</sup> on **s0**, corresponding to the H–H vibration.

**Calculated Vibrational Frequencies for Al–H Species.** The  $\nu(\text{Al–H})$  stretching frequencies were calculated (Table 5) and compared with experimental values (1860–1870 and 1900–1920 cm<sup>-1</sup>).<sup>40</sup> Because Al<sub>IVb</sub> is reconstructed in the most stable structures, both dissociations on Al<sub>III</sub> and Al<sub>IVb</sub> lead to the formation of tetrahedral hydrides. There is a significant influence of Al–H···H interactions: when these are absent,  $\tilde{\nu}(\text{Al–H})$  is in the range of 1900–1950 cm<sup>-1</sup>, while the vicinity of protons shifts the Al–H stretching frequency down to values of 1770–1865 cm<sup>-1</sup>. Bridging hydrides on Al<sub>IVa</sub> give rise to Al–H vibrations in the 1250–1460 cm<sup>-1</sup> region, which are not observed by IR spectroscopy because their frequency falls into

**Table 6.** Shift of the Band Center  $\Delta\epsilon$  (in eV) upon Hydration for the Unoccupied Al 3s–3p States and the Occupied O 2s–2p States with Respect to the s0 Surface<sup>a</sup>

surface	Al <sub>III</sub>	Al <sub>IVb</sub>	O <sub>2a</sub>	O <sub>2a'</sub>	O <sub>2b</sub>	O <sub>3a</sub> /O <sub>3a'</sub>	O <sub>3b</sub>
s1c	+1.03	+0.34	+0.98	−1.53	−0.69	+0.46/+0.33	+0.27
s1a	−	−0.70	−0.31	−2.75	−1.58	−0.42/−0.62	−0.59
s2c	+1.29	−	−	−1.73	−0.22	+0.45/+0.40	−
s2b	−	+0.24	−	−2.24	−1.12	+0.50/+0.50	+0.20
s2b'	−	+0.41	+0.81	−1.53	−0.60	+0.47	+0.28
s3c	+1.83	−	−	−1.40	−	−	−

<sup>a</sup>See also Figure S11 for the full PDOS representation.

the range of Al<sub>2</sub>O<sub>3</sub> lattice vibrations. We can therefore assign the experimentally observed bands to tetrahedral hydrides with and without Al–H···H interactions, respectively. Because these hydrides can be formed on Al<sub>III</sub> and Al<sub>IVb</sub> sites, they are indistinguishable in the final state, especially when considering proton migration. While the band at 1900 cm<sup>−1</sup> would also be compatible with hydrides on the (100) termination, their existence is unlikely because they are not stable (endoenergetic reaction).

## DISCUSSION

We have presented a large set of experimental and theoretical results, which give a detailed picture of the reactivity of the  $\gamma$ -Al<sub>2</sub>O<sub>3</sub> surface as a function of its hydroxylation. In view of the unexpected effect of hydration on reactivity, the discussion aims at rationalizing the results at a molecular level.

**Acidity and Basicity of Surface Sites As a Function of Hydration: PDOS Analysis.** An approach to characterize the intrinsic reactivity of surface Al and O sites is to consider the density of states projected on Kohn–Sham orbitals [projected density of states, (PDOS)]. The PDOS on 3s and 3p orbitals of surface Al (lowest unoccupied bands in alumina) gives information about the Lewis acidity of the respective Al atoms. The Lewis basicity of the surface O atoms can be evaluated in a similar way using the PDOS of the surface oxygen 2s and 2p orbitals that are the constituents of the highest occupied bands in solids.

A simplified descriptor of these projected bands is their energy-weighted mean  $\epsilon$  (band average or band center):

$$\epsilon = \frac{\sum \text{PDOS}(E_i) \cdot E_i}{\sum \text{PDOS}(E_i)}$$

where PDOS( $E_i$ ) is the PDOS on a given set of atomic orbitals in an energy interval [ $E_i, E_i + \Delta E$ ] (a value of 0.0175 eV was chosen for  $\Delta E$ ). For Al, the sum comprises the unoccupied 3s and 3p states which lie in a range of −1 to +10 eV, while for O the sum over the highest occupied 2s and 2p states falls into the range of −10 to 0 eV. To allow a comparison between surfaces, the vacuum potential (plane-averaged electrostatic potential of an electron in the  $z$ -direction of the unit cell far from the surface) of the respective surfaces was used as reference value. The shift of the Al and O band centers ( $\Delta\epsilon$ , see Table 6) on a partially hydroxylated surface  $si$  with respect to  $s0$  is defined as

$$\Delta\epsilon = \epsilon(si) - \epsilon(s0)$$

A positive value of  $\Delta\epsilon$  indicates a decrease of the Lewis acidity, while a downshift indicates a higher Lewis acidity. For O atoms, an upshift is associated with a higher basicity, while a downshift means that the basicity is lower than on  $s0$ .

**Lewis Acidity of Al<sub>III</sub> Sites.** On the fully hydrated  $s0$  surface, Al<sub>III</sub> clearly shows the features with the lowest energy with a band center at  $\epsilon = -0.72$  eV, underlining its superior Lewis acidity, compared to Al<sub>IVb</sub> (−0.24 eV) and Al<sub>IVa</sub> (+0.03 eV), see Figure S10.<sup>50</sup> The PDOS for Al<sub>III</sub> is profoundly affected by adsorption of the first water molecule on Al<sub>IVa</sub> (yielding the metastable  $s1c$ ), as evidenced by the large shift to higher energy ( $\Delta\epsilon = 1.03$  eV) for the vacant Al sp band and the disappearance of the main low-energy feature at ca. −1.5 eV (see Figure S11 for the full PDOS representation). Adsorption of an additional H<sub>2</sub>O on Al<sub>IVb</sub> (yielding  $s2c$ ), followed by surface reconstruction, further shifts the Al sp band upward by ca. 0.3 eV, and a third H<sub>2</sub>O on Al<sub>IVa</sub> (yielding  $s3c$ ) continues this trend with an additional upshift of ca. 0.5 eV. When the Lewis acidity of the Al<sub>III</sub> site is measured by the adsorption energy of N<sub>2</sub> and CO (Table 2), it decreases with hydroxylation of neighboring Al sites, in agreement with this upward shift.

**Lewis Acidity of Al<sub>IVb</sub> Sites.** A notable feature on this site is that the adsorption energy of CO and N<sub>2</sub> first increases counterintuitively upon hydroxylation ( $s1a$ ) but then decreases again upon further hydroxylation ( $s2b'$ , Table 2). In fact, the average of the Al<sub>IVb</sub> band on  $s1a$  is shifted to lower values (by ca. 0.8 eV), compared to  $s0$  (Table 6), thus indicating a higher intrinsic Lewis acidity of Al<sub>IVb</sub> when Al<sub>III</sub> is hydroxylated. This shift brings the center of the Al<sub>IVb</sub> PDOS to an energy ( $\epsilon = 0.94$  eV) close to that of Al<sub>III</sub> on the hypothetical  $s0$  ( $\epsilon = -0.72$  eV, see Figure S11). This is consistent with the stronger adsorption of CO and N<sub>2</sub> on Al<sub>IVb</sub> on  $s1a$ , compared to  $s0$ . This effect is strongly dependent on the position of the OH group since on  $s1c$ , where the Al<sub>IVa</sub> is hydroxylated instead, the center of the Al<sub>IVb</sub> band is shifted to higher energy (by ca. 0.3 eV). The adsorption of a second OH on Al<sub>IVa</sub>, leading to  $s2b$  and  $s2b'$  has no further influence. The shifts are strongly dependent on the position of the OH group(s). Overall, the acidity of Al<sub>IVb</sub> decreases as follows:  $s1a > s0 > s2b > s1c > s2b'$ .

**Lewis Basicity of O<sub>2a</sub>.** The Lewis basicity of O<sub>2a</sub> is strongly increased by the presence of OH on Al<sub>IVa</sub> ( $s1c$ , upshift of the O band center by 0.98 eV) but decreased when OH is on Al<sub>III</sub> ( $s1a$ , downshift of the O band center by 0.31 eV, see Table 6). When Al<sub>III</sub> and Al<sub>IVa</sub> are simultaneously hydroxylated ( $s2b'$ ), the dominating increased basicity from  $s1c$  is conserved. Overall, the basicity of O<sub>2a</sub> decreases as follows:  $s1c \approx s2b' > s0 > s1a$ .

**Lewis Basicity of O<sub>2a'</sub>.** In all cases, this O site becomes tricoordinate upon protonation, which leads to a strong decrease of its basicity.

**Lewis Basicity of O<sub>3a</sub>.** The Lewis basicity of O<sub>3a</sub> (and O<sub>3a'</sub>) is increased when water is adsorbed on Al<sub>IVa</sub> of  $s1c$  and  $s2c$  (upshift of the O band center by ca. 0.3–0.5 eV, see Table 6). Additional hydration of Al<sub>IVb</sub> ( $s2c$ ) has little effect on the basicity. In contrast, hydration of Al<sub>III</sub> ( $s1a$ ) leads to a reduced

basicity of O<sub>3a</sub>, as found for O<sub>2a</sub> (downshift of the O band center by 0.4–0.6 eV). Overall, the basicity of O<sub>3a</sub> decreases as follows: **s2c** ≈ **s1c** > **s0** > **s1a**.

However, these DOS evaluated in the initial structures of the surfaces do not allow understanding quantitatively all the reactivity features. Although the analysis clearly shows, for example, the enhanced basicity of O<sub>2a</sub> and O<sub>3b</sub> on the **s1c** surface, it does not explain why the nonadjacent site Al<sub>III</sub>O<sub>3a</sub> is more reactive than the adjacent site Al<sub>III</sub>O<sub>2a</sub> on this surface.

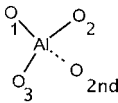
**Origin of the Influence of Hydration on the Al and O Band Centers.** The general trend is that the hydroxylation on Al<sub>IVa</sub> (**s1c** surface) gives less acidic Al<sub>III</sub> atoms and more basic O atoms, while in contrast, hydroxylation of Al<sub>III</sub> (most stable **s1a** surface) gives more acidic Al<sub>IVb</sub> and less basic O atoms. In fact, the heterolytic dissociative adsorption of water produces OH (δ<sup>-</sup>) and H (δ<sup>+</sup>) charged species on the alumina surface as evidenced by Bader charges on OH and H fragments, which are -0.83 and +0.65, respectively. This induces a shift of the energy levels of the Al 3sp and O 2sp states of the neighboring atoms. The OH (δ<sup>-</sup>) groups shift the levels of neighboring O atoms upward because of Coulomb repulsion. For instance, on **s1c**, the presence of the OH (δ<sup>-</sup>) group on Al<sub>IVa</sub> shifts up the level of the attached O<sub>2a</sub> or O<sub>3a</sub> (distance to OH of ca. 2.6 Å) and thus enhances their Lewis basicity. In contrast, the presence or interaction of H (δ<sup>+</sup>) stabilizes the negatively charged oxygen, thus explaining the strong downshifts of the levels (see O<sub>2a</sub>/O<sub>2b</sub> in Table 6). On **s1a** the H (δ<sup>+</sup>) on O<sub>2a</sub> interacting via hydrogen bonding with O<sub>2b</sub> induces a downshift of the Al 3sp states of Al<sub>IVb</sub> thus increasing its Lewis acidity.

**Acidity and Basicity of Surface Sites as a Function of Hydration: Adsorption of Probe Molecules.** When analyzing the PDOS on surface Al atoms, a qualitative agreement is obtained with N<sub>2</sub> and CO adsorption energies, but, there is no quantitative correlation with the average band shift of the Al PDOS. For Al<sub>III</sub>, for example, there is a strong shift of ε<sub>AL</sub> from **s0** to **s1c**, while the adsorption energy difference is small (4 kJ mol<sup>-1</sup> for CO and 11 kJ mol<sup>-1</sup> for N<sub>2</sub>). In contrast between **s1c** and **s2c**, the shift of ε<sub>AL</sub> is smaller, while the decrease of adsorption energy is higher (24 kJ mol<sup>-1</sup> for CO and 31 kJ mol<sup>-1</sup> for N<sub>2</sub>).

From a geometric point of view, it is clear that an O atom from the second layer of alumina is partially coordinated to Al<sub>III</sub> for **s1c**, **s2c**, and **s3c** and that the strength of this interaction increases with the OH coverage; such interaction being absent on **s0** (Table 7). In fact, Al<sub>III</sub> is significantly pyramidalized

**Table 7. Structural Parameters for Surfaces with a Free Al<sub>III</sub> Site**

	Ω(O <sub>1</sub> -O <sub>2</sub> -O <sub>3</sub> -Al <sub>III</sub> ) [°]	d(Al-O <sub>2nd</sub> ) [Å]
<b>s0</b>	+8.6	2.76
<b>s1c</b>	-13.1	2.09
<b>s2c</b>	-24.6	1.97
<b>s3c</b>	-24.9	1.93
<b>bulk</b>	-	1.80



inward the alumina bulk on **s2c** and **s3c**. The Al–O distance for tetrahedral Al in the bulk of γ-Al<sub>2</sub>O<sub>3</sub> is ca. 1.8 Å, therefore the Al<sub>III</sub> is approaching this coordination, and it can be considered as an intermediate between Al<sub>III</sub> (as found on **s0**) and Al<sub>IV</sub>. In the case of CO, adsorption structures are very similar on all three surfaces, as evidenced from the Al–C and C–O distances (Table S1). The Al<sub>III</sub> moiety is pyramidalized outwards (Ω =

+20 to +26°) and the second-layer O atom is not any longer coordinated to Al<sub>III</sub>. Hence in the case of the hydrated terminations, adsorption is accompanied by a strong deformation at the Al adsorption site, which must be associated with an energy cost.

This can be evaluated by a decomposition of the adsorption energy of CO on the various **si** terminations into deformation energy  $E_{\text{def}}$  and interaction energy  $E_{\text{int}}$  components (Table 8):

$$E_{\text{def}}(\text{CO}) = E(\text{CO})_{\text{ads}} - E(\text{CO})$$

$$E_{\text{def}}(\text{si}) = E(\text{si})_{\text{ads}} - E(\text{si})$$

$$E_{\text{int}} = E(\text{CO} + \text{si}) - E_{\text{def}}(\text{CO}) - E_{\text{def}}(\text{si})$$

**Table 8. Energy Decomposition Scheme for the Adsorption of CO and N<sub>2</sub> on the Various Al Sites of the s0, s1, and s2 Surfaces**

molecule	ads. site	surface	$E_{\text{ads}}$	$E_{\text{def}}(\text{si})^a$	$E_{\text{int}}^b$
			[kJ mol <sup>-1</sup> ]		
CO	III	<b>s0</b>	-74	+9	-83
		<b>s1c</b>	-70	+26	-96
		<b>s2c</b>	-38	+68	-106
	IVb	<b>s0</b>	-45	+11	-55
		<b>s1a</b>	-60	+11	-71
		<b>s1c</b>	-55	+15	-70
		<b>s2b</b>	-38	+13	-51
		<b>s2b'</b>	-45	+16	-60
	V	<b>s0</b>	-37	+8	-45
	N <sub>2</sub>	III	<b>s0</b>	-41	+7
<b>s1c</b>			-30	+19	-49
<b>s2c</b>			-6	+1	-7
IVb		<b>s0</b>	-15	+5	-20
		<b>s1a</b>	-28	+8	-37
		<b>s1c</b>	-19	+7	-26
		<b>s2b</b>	-12	+5	-17
		<b>s2b'</b>	-14	+6	-20
V		<b>s0</b>	-11	+5	-16

<sup>a</sup>Calculated with **si** frozen in the geometry of the adsorption state:  $E_{\text{def}}(\text{si}) = E(\text{si})_{\text{ads}} - E(\text{si})$ . <sup>b</sup> $E_{\text{int}} = E(\text{CO} + \text{si}) - E_{\text{def}}(\text{CO}) - E_{\text{def}}(\text{si})$ .

where  $E(\text{CO})_{\text{ads}}$  and  $E(\text{si})_{\text{ads}}$  are the energies of CO and of the **si** surface in the geometry that these subsystems adopt in the complex between the **si** surface and the CO molecule.

In all cases, the deformation energy for CO is negligible. However, that of the surface increases from **s0** to **s1c** and is considerably higher for **s2c**. This is clearly related to the relatively strong bond between Al<sub>III</sub> and a second-layer O atom (1.97 Å) on **s2c** that needs to be broken for Al<sub>III</sub> to become reactive and to coordinate a Lewis base. The same analysis also explains why N<sub>2</sub> is adsorbed on **s0** and **s1c** and not on **s2c** or **s3c**. On the more hydrated **s2c** and **s3c** surfaces, the deformation energy is prohibitively high and cannot be compensated by the weak Lewis acid–base interaction with N<sub>2</sub>.

Note, that experimental evidence for the deformation of Al surface sites upon CO adsorption has been found by IR spectroscopy. With increasing CO pressure, bands in the 1000–1050 cm<sup>-1</sup> region gradually disappear.<sup>46</sup> These adsorptions have been attributed to Al–O stretching modes of truncated surface tetrahedral Al sites, i.e., Al<sub>III</sub> sites, which become bulk-like Al<sub>IV</sub> upon coordination of CO. The intensity

of these surface Al–O modes increases with pretreatment temperature of alumina and hydration annihilates them, as already earlier reported by Lavalley.<sup>60</sup>

The analysis of the surface deformation is complemented by examining the PDOS for Al<sub>III</sub> sites in the deformed geometry of the alumina surface after adsorption, but with CO removed (Figure 6). The band center is shifted to lower energy, and the

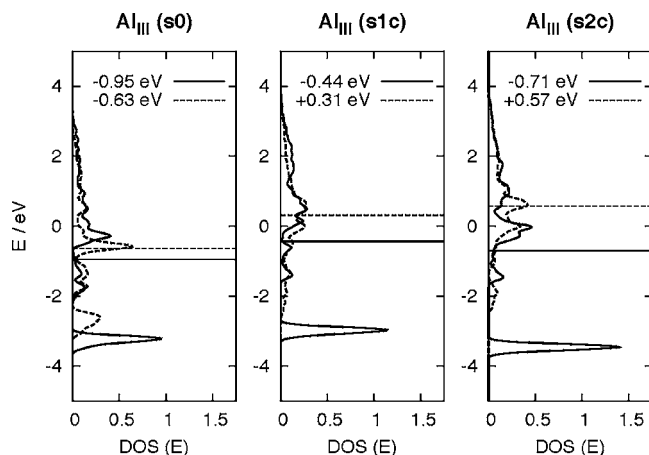


**Figure 6.** DOS projected on the 3s–3p states of Al<sub>III</sub> for **s0**, **s1c**, and **s2c** surfaces for the fully relaxed surfaces (dashed line) and in the geometry of the CO adsorption complex (but with CO removed, full line). A horizontal line indicates the position of the weighted average of each band.

lowest energy feature (corresponding to the LUMO) is much more developed than on the relaxed surface, confirming that the distortion of the surface is necessary to reach the “right” pyramidalization and associated Lewis acidity to interact optimally with the probe molecule. The shift of the band center from its initial value is clearly highest on **s2c**, thus confirming that Al<sub>III</sub> on this surface must undergo the strongest structural change to achieve a reactive structure. Interaction energy values ( $E_{\text{int}}$ ) confirm that **s1c** and **s2c**, at the cost of proper geometric distortions, can be as reactive as **s0**. Hence, the slightly lower Lewis acidity of **s1c** compared to **s0** is due to the small energy cost for reaching a reactive configuration, because only a relatively weak interaction with the second-layer O is initially present on **s1c**. In contrast, on **s2c** (and conversely on **s3c**), where this interaction is stronger, the associated cost is much higher, thus rationalizing the lower Lewis acidity of Al<sub>III</sub>. The Al<sub>III</sub> of **s1c**, despite a coordination in between a true Al<sub>III</sub> and a Al<sub>IV</sub>, has thus a reactivity similar to Al<sub>III</sub> of the fully dehydrated **s0**. Chemically, it can hence be considered as a “true” Al<sub>III</sub>.

One might expect that structural effects, which played a decisive role on Al<sub>III</sub>, do not affect the adsorption of CO and N<sub>2</sub> on Al<sub>IVb</sub>. Indeed, the decomposition of the adsorption energy (Table 8) shows that the deformation energy of the surface upon adsorption is small and similar in all cases. On the other hand, the interaction energy between the surface and CO/N<sub>2</sub> fragments is typically higher in the case of **s1a** and **s1c**, thus indicating a higher Lewis acidity of the Al site and confirming the result obtained from the PDOS analysis.

**Effect of Hydration on the Stability of Al–H and Al–CH<sub>3</sub> Species.** While the difference in reaction energy on a given Al<sub>i</sub>O site and surface, when comparing the formation of Al–H and Al–CH<sub>3</sub>, is not affected by hydration (see the last

section of the Discussion for analysis), the reaction energy itself is. On the most reactive site (adjacent Al<sub>III</sub>O<sub>2a</sub>), compared to the fully dehydrated **s0**, the formation of Al–H and Al–CH<sub>3</sub> is only slightly disfavored at low water coverage ( $\Delta = +19/+21$  kJ mol<sup>-1</sup> with 1 H<sub>2</sub>O per unit cell, **s1c**, 3 OH nm<sup>-2</sup>) but much less favorable at an intermediate water coverage ( $\Delta = +74/+71$  kJ mol<sup>-1</sup> with 2 H<sub>2</sub>O per unit cell, **s2c**, 6 OH nm<sup>-2</sup>). On **s1c** the decrease of the Lewis acidity of Al<sub>III</sub> is probably compensated by an increased basicity of O<sub>2a</sub> (see Table 5), yielding only a small attenuation of the dissociation energy since both Al and O are involved. While hydrogen bonds are more numerous, they become weaker with increasing hydration (compare structures 1–3 in Tables 3 and 4). The significant destabilization on **s2c** is related to the protonation of a less basic tricoordinate atom in the second Al<sub>2</sub>O<sub>3</sub> layer. Compared to dissociation on the adjacent Al<sub>III</sub>O<sub>2a</sub> site, the effect of hydration on the reactivity of CH<sub>4</sub> and H<sub>2</sub> on the nonadjacent Al<sub>III</sub>O<sub>3a</sub> site is more unexpected; while the reaction is only slightly favorable on **s0** for H<sub>2</sub> and slightly endoenergetic for CH<sub>4</sub>, it is significantly more favorable on the partially hydrated **s1c** and **s2c** surfaces for both molecules ( $\Delta = -40$  to  $-48$  kJ mol<sup>-1</sup>). In the final state, after dissociation of CH<sub>4</sub>, the proton is attached to a dicoordinate O atom, while it is on a tricoordinate O on **s0**. This underlines the crucial role of oxygen basicity for the dissociation of CH<sub>4</sub>. Water can be regarded as a promoter for the dissociation on Al<sub>III</sub>–O<sub>3a</sub>, because the occupation of both Al<sub>IVa</sub> by a bridging OH group leads to a weakening of the Al<sub>IVa</sub>–O<sub>3a</sub> bond, thus enabling the formation of the more basic dicoordinate O (not counting the attached proton) in the final state. Indeed, on **s1c** and **s2c**, the Al<sub>IVb</sub>–O<sub>3a</sub> bond is elongated by 0.07 and 0.03 Å from the increased Al coordination (IV to V), compared to **s0**.

For dissociation on the Al<sub>IVb</sub>O<sub>3b</sub> site a similar effect is found: On both **s1c** and **s2b**, the dissociation of CH<sub>4</sub> and H<sub>2</sub> is favored over that on the nonhydrated **s0** surface, especially for low water coverage ( $\Delta = -36/-39$  on **s1c** and  $-10/-10$  on **s2b'** for H<sub>2</sub>/CH<sub>4</sub>, respectively, structures 8, 9 and 11 in Tables 3 and 4). The process is here however more complex since it is associated with a reconstruction of Al<sub>IVb</sub> toward a tetrahedral structure. The oxygen O<sub>2a</sub> is more basic on **s1c** and **s2b'** (Table 6) which favors the formation of the new Al<sub>IVb</sub>–O<sub>2a</sub> bond in the reconstruction process. In addition, the basicity of O<sub>3a</sub> is also enhanced. Thus, hydroxylation of Al<sub>IVa</sub> favors the dissociation of CH<sub>4</sub> or H<sub>2</sub> on Al<sub>IVb</sub>.

Finally, note that the adsorption of both molecules on Al<sub>IVa</sub> is barely affected by hydration. But overall, water is a key ingredient for reactivity, and it is very important to consider Lewis acid–base pairs as reactive sites, rather than focusing only on the Lewis acidity of Al.

#### Effect of Hydration on the TS Structures and Energies for CH<sub>4</sub> and H<sub>2</sub> dissociation.

The absolute TS energies on given Al–O sites vary with hydration, but the difference in TS energy between CH<sub>4</sub> and H<sub>2</sub> is almost constant (ca. 30 kJ mol<sup>-1</sup> lower for H<sub>2</sub>), except on the nonadjacent Al<sub>III</sub>O<sub>3a</sub> sites where the barrier is lowered by ca. 50 kJ mol<sup>-1</sup>. The optimal geometry in the TS requires a deformation of the substrate and the surface, as seen in the case of CO and N<sub>2</sub> coordination, but here, in addition, the O site also needs to be deformed. This deformation induces a reduced energy gap between the lowest unoccupied Al levels and the highest occupied O levels, hence a more reactive Al<sub>i</sub>O pair, as evident from the shift of the band centers ( $\Delta\epsilon$ ) of the occupied O and unoccupied Al levels (Table 9 and Figures S12–S14). Such Al<sub>i</sub>O pairs can be

Table 9. Decomposition of the TS Energy for H<sub>2</sub> and CH<sub>4</sub> Dissociation on (Al<sub>2</sub>O)<sup>a</sup>

molecule	site	surface	$E_{\text{TS}}$	$E_{\text{def.}}(\text{XH})^b$	$E_{\text{def.}}(\text{si})$	$E_{\text{int}}^{\ddagger}$	$\Delta\epsilon(\text{Al})$	$\Delta\epsilon(\text{O})$	
			[kJ mol <sup>-1</sup> ]						[eV]
H <sub>2</sub>	Al <sub>III</sub> O <sub>2a</sub>	s0	34	75	33	-74	-0.40	+0.59	
		s1c	43	65	35	-57	-0.68	+0.18	
		s2c	85	89	64	-68	-1.02	(+2.24) <sup>c</sup>	
	Al <sub>III</sub> O <sub>3a</sub>	s0	27	69	77	-119	-0.57	+1.31	
		s1c	-4	22	52	-78	-0.80	+1.48	
		s2c	55	22	102	-68	-0.91	+1.67	
	Al <sub>IVa</sub> O <sub>2a</sub>	s0	76	77	54	-55	-1.23	+0.74	
		Al <sub>IVb</sub> O <sub>2b</sub>	s0	43	75	34	-66	-0.66	+0.62
			s0	61	73	50	-61	-0.76	+0.91
	Al <sub>IVb</sub> O <sub>3b</sub>	s1c	57	4	82	-32	-0.26	+2.71	
		s2b'	s0	75	9	103	-37	-0.44	+1.66
			s0	64	169	47	-151	-0.48	+0.63
CH <sub>4</sub>	Al <sub>III</sub> O <sub>2a</sub>	s1c	74	152	51	-129	-0.77	+0.18	
		s2c	116	178	81	-144	-1.20	(+2.16) <sup>c</sup>	
		s0	86	244	100	-258	-0.65	+1.46	
	Al <sub>III</sub> O <sub>3a</sub>	s1c	45	174	94	-223	-0.98	+1.77	
		s2c	103	174	151	-223	-1.18	+1.98	
		s0	116	155	71	-110	-1.41	+0.76	
	Al <sub>IVa</sub> O <sub>2a</sub>	s0	79	154	47	-122	-0.79	+0.62	
		Al <sub>IVb</sub> O <sub>2b</sub>	s0	98	158	86	-128	-0.92	+0.93
			s0	72	10	99	-38	-0.41	+2.90
	Al <sub>IVb</sub> O <sub>3b</sub>	s1c	72	10	99	-38	-0.41	+2.90	
		s2b'	90	19	127	-56	-0.57	+1.96	

<sup>a</sup>Shift of the band center ( $\Delta\epsilon$ ) of the unoccupied Al 3s–3p states and the occupied O 2s–2p states in the TS with respect to the fully relaxed geometry. See also the full PDOS representation in Figures S12–15. <sup>b</sup>Calculated with XH (X = H, CH<sub>3</sub>) frozen in the geometry of the TS:  $E_{\text{def.}}(\text{XH}) = E(\text{XH})_{\text{TS}} - E(\text{XH})$ . <sup>c</sup>Calculated with *si* frozen in the geometry of the TS:  $E_{\text{def.}}(\text{si}) = E(\text{si})_{\text{TS}} - E(\text{si})$ . <sup>d</sup> $E_{\text{int}}^{\ddagger} = E^{\ddagger} - [E_{\text{def.}}(\text{XH}) + E_{\text{def.}}(\text{si})]$ . <sup>e</sup>O<sub>2a</sub> is initially protonated.

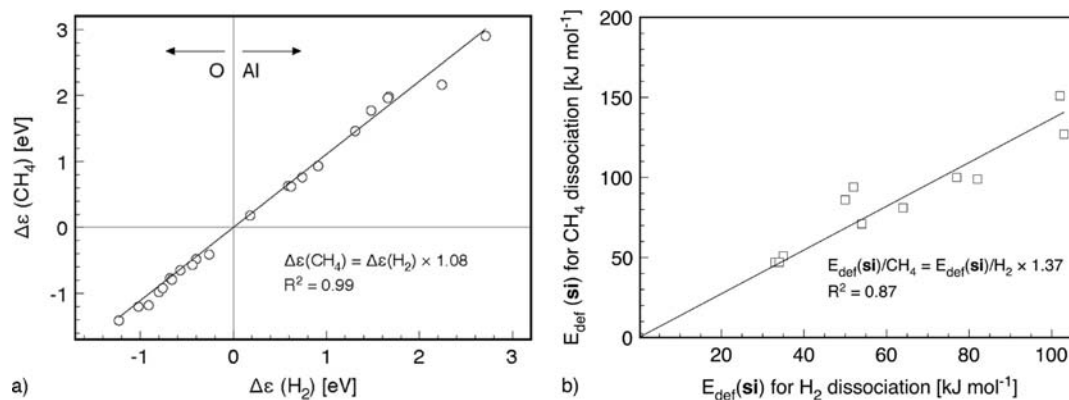


Figure 7. Plot of the (a) shifts of the band centers ( $\Delta\epsilon$ ) and (b) deformation energy,  $E_{\text{def}}(\text{si})$ , for CH<sub>4</sub> vs H<sub>2</sub> dissociation.

compared to homogeneous acid–base systems such as sterically hindered molecules containing B,P pairs. These so-called “frustrated Lewis acid–base pairs” afford the heterolytic splitting of H<sub>2</sub> in mild conditions.<sup>61–63</sup> The shift of the band centers for the TSs is very similar for CH<sub>4</sub> and H<sub>2</sub> on given sites (see the PDOS representation in the SI) and indeed a plot of these band center shifts for CH<sub>4</sub> dissociation vs H<sub>2</sub> dissociation TSs yields an almost perfect linear correlation with a slope of 1.08 (Figure 7a). This means that for CH<sub>4</sub> activation the band centers, both for Al and O, are slightly more shifted to lower and higher energy, respectively, thus creating a more reactive frustrated Al<sub>2</sub>O pair by increasing the “HOMO–LUMO gap” to adapt to the less reactive CH<sub>4</sub>. In addition the longer C–H bond demands a more elongated Al–O bond in the TS. The formation of this more reactive pair requires a stronger

deformation of the surface, and this additional cost is quite significant, as shown in Table 9 and graphically represented in Figure 7b. While there is only a fair correlation between the deformation energies,  $E_{\text{def}}(\text{si})$  in the TS is on average 1.4 times higher for the dissociation of CH<sub>4</sub> compared to H<sub>2</sub>.

We now analyze the origin of the TS energy in more detail by examining the energy decomposition scheme for the reaction of H<sub>2</sub> on the s0 surface because its deformation induces less structural change than for CH<sub>4</sub> and is therefore easier to understand. The deformation energy of H<sub>2</sub> is almost the same for all TSs (69–77 kJ mol<sup>-1</sup>), independent of the reaction sites (Table 9), and is associated with an elongation of the H–H bond from 0.74 to ca. 1.0 Å (see Figure S9 and Table S4). The difference between adjacent Al<sub>2</sub>O sites arises mainly from the deformation energy of the surface, which is ca. 20 kJ

$\text{mol}^{-1}$  higher for  $\text{Al}_{\text{IVa}}, \text{O}_{2\text{a}}$  and  $\text{Al}_{\text{IVb}}, \text{O}_{3\text{b}}$  than for the  $\text{Al}_{\text{III}}, \text{O}_{2\text{a}}$  and  $\text{Al}_{\text{IVb}}, \text{O}_{2\text{a}}$  sites. However, the highest deformation energy for the surface is found for the nonadjacent  $\text{Al}_{\text{III}}, \text{O}_{3\text{a}}$  site. The  $\text{Al}_{\text{III}}$  is more pyramidalized [ $\sum\alpha(\text{CH}_3) = 343.8$  compared to 349.4 for the adjacent site] and six Al–O bonds are elongated vs only one for the adjacent site. This significant deformation of the surface ( $E_{\text{def}} = 77 \text{ kJ mol}^{-1}$ ) is necessary to form a reactive Al–O pair, as suggested by the PDOS (Table 9). Both the Lewis acidity of Al and the Lewis basicity of O are increased in the TS. Note the strong shift in the center of the O 2s,2p band ( $\Delta\epsilon$ , +1.31 eV) that is necessary to enhance the basicity of the initially unreactive  $\text{O}_{3\text{a}}$  atom. As a result, the interaction energy is much higher on the nonadjacent site compared to the adjacent sites, and the TS energy is low, despite the high deformation required. This is probably also related to the more linear 4-electron-3-center TS on the nonadjacent site (H–H–O angle: 170.2 vs 143.2° for the activation on adjacent Al–O sites), leading to a better overlap between orbitals (Figure 5).

Comparing  $\text{CH}_4$  and  $\text{H}_2$  dissociation, the deformation energy of the surface (by 14–36  $\text{kJ mol}^{-1}$ ) is higher on all sites, since the longer C–H bond demands a more elongated Al–O bond and a more distorted Al atom in the TS. But the most significant contribution is of course the more difficult deformation of the tetrahedral  $\text{CH}_4$  molecule, compared to the linear  $\text{H}_2$ . On the nonadjacent  $\text{Al}_{\text{III}}, \text{O}_{2\text{a}}$  site, the deformation energy for  $\text{CH}_4$  site is higher by ca. 90  $\text{kJ mol}^{-1}$  compared to the adjacent site, while for  $\text{H}_2$  there is essentially no difference. In fact,  $\text{CH}_4$  requires a larger distortion of its geometry, while the linear  $\text{H}_2$  molecule can easily adopt the necessary linear arrangement of the O–H–X moiety (X = H,  $\text{CH}_3$ ) in the TS.

After examining the hypothetical fully dehydrated **s0** surface, we now address the TSs on  $\text{Al}_{\text{III}}$  and  $\text{Al}_{\text{IV}}$  sites on the more realistic hydrated surfaces.

**Adjacent  $\text{Al}_{\text{III}}, \text{O}_{2\text{a}}$  Site.** As found on **s0**, the distortion in the TS enhances both the Lewis acidity of Al and basicity of O, and the associated band shifts are similar for  $\text{H}_2$  and  $\text{CH}_4$  (Table 9 and Figure S12). For both molecules, the shift of the  $\text{Al}_{\text{III}}$  band center ( $\Delta\epsilon$ ) to lower energy is slightly larger on **s1c** than on **s0**, indicating that in order to be reactive toward  $\text{H}_2/\text{CH}_4$  a rather small deformation of the  $\text{Al}_{\text{III}}$  on the **s1c** surface is necessary, compared to **s0**. On the other hand a rather large shift (>1 eV) is found on **s2c**, as already seen in the case of CO and  $\text{N}_2$  adsorption. Indeed the outward pyramidalization of the Al atom is hindered since it requires breaking a bond to a second-layer O atom on **s2c**.

On all surfaces the  $\text{O}_{2\text{a}}$  band center is shifted to higher energy in the TS.  $\text{O}_{2\text{a}}$  is initially more basic on **s1c** because  $\text{Al}_{\text{IVa}}$  is hydroxylated (vide supra, Table 6), therefore  $\Delta\epsilon$  is much smaller than on **s0**. The enhanced basicity of  $\text{O}_{2\text{a}}$  is a key ingredient to keep a moderate deformation of the surface and a low barrier on **s1c** despite the less acidic Al atom. On **s2c** the shift is very large (more than 2 eV) because the initially protonated  $\text{O}_{2\text{a}}$  atom loses its proton in the TS, thus drastically increasing its basicity. Overall, the deformation energy of the surface,  $E_{\text{def}}(\text{si})$ , reflects the shifts of the band centers, in particular that of Al, with a much more difficult deformation of **s2c**, as observed for  $\text{N}_2$  and CO.

The deformation energy of  $\text{H}_2/\text{CH}_4$  in the TS (Table 9) follows the elongation of the  $\text{H}_1\text{--H}_2/\text{C--H}$  bond but is not much affected by hydration. The overall energetic cost associated with the deformation of the surface and  $\text{H}_2/\text{CH}_4$  results in a small barrier increase on **s1c**, compared to **s0**, but a strong destabilization on **s2c**.

**Nonadjacent  $\text{Al}_{\text{III}}, \text{O}_{3\text{a}}$  Site.** The main feature calculated for the nonadjacent  $\text{Al}_{\text{III}}, \text{O}_{3\text{a}}$  site is clearly the low barrier on **s1c**: For  $\text{H}_2$  it is even barrierless when starting from separated reactants and associated with a negligible barrier of only 11  $\text{kJ mol}^{-1}$  when starting from the preadsorption state. The trend for the  $\text{Al}_{\text{III}}$  band center is rather similar to that on the adjacent  $\text{Al}_{\text{III}}, \text{O}_{2\text{a}}$  site, indicating that to reach a reactive geometry in the TS, a small deformation of  $\text{Al}_{\text{III}}$  is necessary on **s1c** but a large one on **s2c**. As found on **s0**, the shift of the O band center to higher energy is strong on the hydrated surfaces, although the basicity of  $\text{O}_{3\text{a}}$  is initially increased on **s1c** and **s2c** (vide supra, Table 6), and it becomes even more pronounced in the TS where we find a significantly higher basicity than on **s0** (Figure S13). It is indeed comparable to that of  $\text{O}_{2\text{a}}$  on the adjacent site in the TS (Figure S12). Hydroxylation on  $\text{Al}_{\text{IVa}}$  combined with the deformation in the TS brings  $\text{O}_{2\text{a}}$  and  $\text{O}_{3\text{a}}$  to the same level of reactivity. The higher O basicity for  $\text{O}_{3\text{a}}$  on **s1c** compared to **s0** allows reaching an earlier TS, compared to the adjacent sites, with a smaller elongation of the H–H/C–H bond and a highly reduced  $\text{H}_2/\text{CH}_4$  deformation energy on the hydrated surfaces. On **s1c**, in the case of  $\text{H}_2$ , the sum of the deformation energies of the molecule and the surface is small (72  $\text{kJ mol}^{-1}$  lower than on **s0**), so that the barrier is very low, despite the reduced interaction energy in the TS. The compromise between deformation and interaction is optimal in this case. Note that almost the same situation is found for  $\text{CH}_4$  (76  $\text{kJ mol}^{-1}$ ).

In summary, the TS energy on the nonadjacent ( $\text{Al}_{\text{III}}, \text{O}_{3\text{a}}$ ) site is governed by the cost for the deformation of both  $\text{H}_2/\text{CH}_4$  and the surface. On **s1c**, both energies are smaller than on **s0**, thus explaining the very low dissociation barrier on this surface, while on **s2c** the large deformation required for the surface “outweighs” the low deformation energy for  $\text{H}_2$ , leading to a higher barrier than on **s0**.

**$\text{Al}_{\text{IVb}}, \text{O}_{3\text{b}}$  Site.** In the TS on the hydrated surfaces, the  $\text{Al}_{\text{IVb}}$  becomes tricoordinate and  $\text{O}_{3\text{b}}$  dicoordinate, a situation reminiscent of the TS on the nonadjacent  $\text{Al}_{\text{III}}, \text{O}_{3\text{a}}$  site. Note, that the shift of the band centers is strongest for O, because the tricoordinate  $\text{O}_{3\text{b}}$  is initially much less basic than the dicoordinate “ $\text{O}_{3\text{b}}$ ” in the TS (Table 9). The decomposition of the TS energy (Table 9) is consistent with the different mechanisms on **s0** and the hydrated surfaces. On the **s0** surface (TS corresponding to H–H or C–H dissociation), both the deformation of the molecule and the surface are equally important. In contrast, on the hydrated **si** surfaces the deformation of the molecule is negligible, but that of the surface is much higher than found for **s0**. In fact, the TS is essentially a reconstruction of the surface to transform an  $\text{Al}_{\text{IVb}}, \text{O}_{3\text{b}}$  pair into a more reactive  $\text{Al}_{\text{III}}, \text{O}_2$  pair. In summary, these effects compensate each other and explain the similar reactivity on **s0** and the hydrated surfaces.

**Origin of the Reactivity Difference between  $\text{H}_2$  and  $\text{CH}_4$ .** Of these two molecules,  $\text{CH}_4$  is more difficult to activate in terms of reaction energies and dissociation barriers by 30–50  $\text{kJ mol}^{-1}$ . This cannot be due to the difference of bond dissociation energies since they are almost identical for H–H and  $\text{CH}_3\text{--H}$  (436 and 435  $\text{kJ mol}^{-1}$ , respectively).<sup>64</sup> In the final state, a similar OH group is formed from  $\text{H}_2$  or from  $\text{CH}_4$ , the only difference being the replacement of an Al–H by an Al– $\text{CH}_3$ . The mean Al–C and Al–H bond dissociation energies (BDE) in the tricoordinate compounds  $\text{Al}(\text{CH}_3)_3$  and  $\text{AlH}_3$  are 281 and 290  $\text{kJ mol}^{-1}$ , respectively.<sup>65</sup> Similarly, high-level calculations for  $\text{Al}(\text{OH})_2\text{H}$  and  $\text{Al}(\text{OH})_2(\text{CH}_3)$  and related compounds show very small differences in Al–C and Al–H

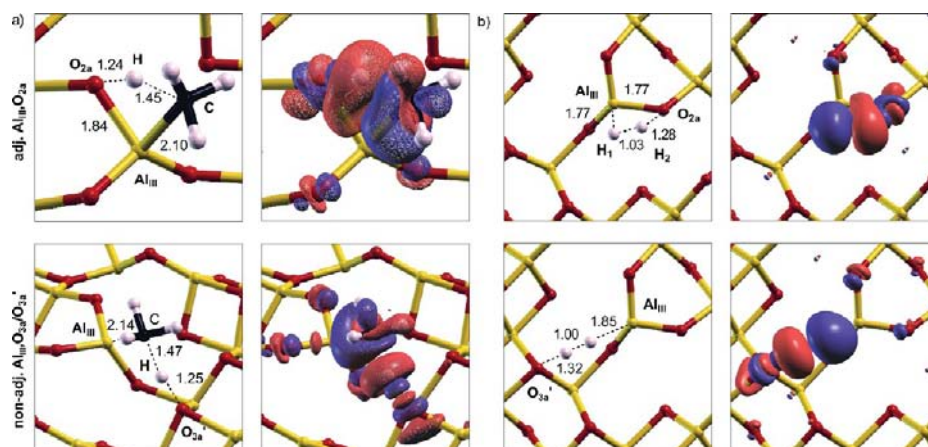
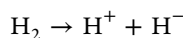
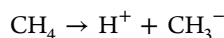


**Figure 8.** Electron density difference maps for the TS for dissociation on the adjacent and nonadjacent  $\text{Al}_{\text{III}}\text{O}$  sites of the  $s_0$  surface. (a)  $\text{CH}_4$  and (b)  $\text{H}_2$ . Blue zones correspond to an increase in electron density and red zones to a depletion. The isocontour corresponds to  $0.03 \text{ \AA}^{-3}$ .

bond energies.<sup>66</sup> The analysis of the differential charge density at the TS shows that the dissociation of  $\text{H}_2$  and  $\text{CH}_4$  on alumina is heterolytic, in contrast to what was found on gas-phase radical clusters.<sup>67,68</sup>

We find a charge accumulation between the carbon (or hydrogen) and the aluminum sites accompanied by a charge depletion on the hydrogen moving toward the oxygen (future proton) (Figure 8). This corresponds to the heterolytic splitting of methane ( $\text{H}_3\text{C } \delta^-/\text{H } \delta^+$ ) or  $\text{H}_2$  ( $\text{H } \delta^-/\text{H } \delta^+$ ) on ( $\text{Al } \delta^+/\text{O } \delta^-$ ), yielding a proton attached to an oxygen atom and formally a methyl anion or a hydride coordinated to an aluminum cation. It is thus not surprising that the difference of TS energy is close to the difference of gas-phase acidities of  $\text{CH}_4$  and  $\text{H}_2$  ( $\Delta_r H^0$ ), which are 1743 and 1675  $\text{kJ mol}^{-1}$ , respectively<sup>69</sup> (this corresponds to a difference of 68  $\text{kJ mol}^{-1}$  or ca. 13  $\text{p}K_a$  units):



Equivalently, this is also consistent with the difference of electron affinity of the H and  $\text{CH}_3$  radical, which are  $-73$  and  $-8 \text{ kJ mol}^{-1}$ , respectively.<sup>70</sup> The formation of an aluminum hydride by heterolytic splitting will hence be easier than that of  $\text{Al}-\text{CH}_3$ . Similar differences in the barriers for the activation of  $\text{H}_2$  and  $\text{CH}_4$  have been reported on  $d^0$  transition metals<sup>71,72</sup> and lanthanide complexes. This has been rationalized in terms of gas-phase acidity for the latter.<sup>73</sup> The difference in gas-phase acidity, or equivalently in electron affinity, thus explains the systematic difference of reactivity between methane and  $\text{H}_2$  on the alumina surface and other surfaces like  $\text{ZnO}$ , where heterolytic splitting has been proposed.<sup>22,74</sup>

**Site Reactivity: What Is the Best Descriptor?** Finally, when looking at all the data, the reactivity of Al sites is not so intuitive, whether looking at the coordination of  $\text{N}_2$  or the splitting of  $\text{H}_2/\text{CH}_4$  as a function of water coverage. In fact, predicting the reactivity of surface sites cannot be reduced to examining their initial coordination geometry in many instances. A better approach is to examine the energy of the average highest occupied (O) as well as the lowest unoccupied (Al) bands projected on surface atoms. This can be seen as a natural extension of HOMO–LUMO in molecular orbital theory<sup>75</sup> and of the d-band model on transition-metal surfaces.<sup>76</sup> The average band positions are shifted by surface

hydroxylation, thus rationalizing the unexpected enhanced adsorption or dissociation on specific sites. Yet, one should still exercise caution when drawing conclusion about the reactivity of surface sites by simply looking at their initial state (coordination and electronic configuration), even using this approach. Instead, the optimal method is to consider their reactive state (structure at the TS or at the adsorption state), where the surface adapts to maximize its interaction with the probe molecule. This is associated with a distortion of the surface and an energetic cost, which contribute to the overall reactivity of sites, giving a more or less strong penalty depending on how rigid the surface has become upon hydroxylation, hence explaining the optimal surface hydroxylation.

## CONCLUSION

The adsorption site density for  $\text{N}_2$ ,  $\text{CH}_4$ , and  $\text{H}_2$  on  $\gamma\text{-Al}_2\text{O}_3$  describes a volcano curve as a function of its pretreatment temperature and water coverage. A similar behavior is observed for the adsorption of  $\text{CH}_4$  and  $\text{H}_2$  on  $\delta\text{-Al}_2\text{O}_3$  but with a higher site density (20–30%). This strongly suggests that the same type of site is present on both aluminas, and it is consistent with what has been recently observed for the adsorption of  $\text{CO}$  and  $\text{H}_2$  on  $\gamma/\delta\text{-Al}_2\text{O}_3$ ,<sup>42</sup> where the difference between these two aluminas has been attributed to the higher crystallinity of the  $\delta$ -phase, leading to a less heterogeneous surface and better-defined adsorption sites.

$\text{N}_2$  adsorbs through coordination to Al Lewis acid sites, while  $\text{CH}_4$  and  $\text{H}_2$  undergo heterolytic dissociation on Al<sub>IV</sub>O Lewis acid–base pairs to form  $\text{Al}-\text{CH}_3$  and  $\text{Al}-\text{H}$  species, respectively. Yet, for all molecules, a minimum pretreatment temperature of 400 °C is required, and the maximum site density is obtained at 700 °C. The reactivity onset above 400 °C clearly shows that dehydration of the surface is a prerequisite to generating reactive sites. Considering that the minor (100) termination is already fully dehydrated at lower temperature (ca. 350 °C), it cannot be involved in the adsorption of these molecules. Indeed, none of its surface Al sites, i.e., five-coordinate  $\text{Al}_V$  or distorted four-coordinate  $\text{Al}_{IV}$ , stabilize  $\text{N}_2$  or yield stable  $\text{Al}-\text{H}$  or  $\text{Al}-\text{CH}_3$  species upon dissociation of  $\text{H}_2$  and  $\text{CH}_4$ , respectively. Thus, the observed reactivity must take place on the major (110) termination, which can expose  $\text{Al}_{III}$  sites, in contrast to alcohol dehydration

reactions, for example, which are proposed to occur on five-coordinate Al of the minor (100) termination.<sup>77</sup>

At high water coverage ( $9 \text{ OH nm}^{-2}$ ), free  $\text{Al}_{\text{III}}$  sites do not exist because OH groups occupy them. At intermediate water coverage ( $6 \text{ OH nm}^{-2}$ ), terminations exposing  $\text{Al}_{\text{III}}$  sites have a surprisingly low energy because the surface is stabilized by reconstruction (formation of tetrahedral Al sites) and the coordination of " $\text{Al}_{\text{III}}$ " by a second-layer oxygen atom. However, the rather high rigidity of this pseudo four-coordinate " $\text{Al}_{\text{III}}$ " prevents its deformation into a "real" and reactive  $\text{Al}_{\text{III}}$  site (as found on the hypothetical fully dehydrated surface), thus dramatically decreasing its Lewis acidity and preventing the coordination of  $\text{N}_2$  or the reaction of methane or hydrogen. Decreasing water coverage ( $3 \text{ OH nm}^{-2}$ ) generates less stable and therefore less probable  $\text{Al}_{\text{III}}$  sites. However, they are much more reactive (Lewis acidic) and readily coordinate  $\text{N}_2$ , with a calculated blue-shift of the N–N vibration in good agreement with experiment. While these  $\text{Al}_{\text{III}}$  sites are also weakly coordinated to subsurface O atoms, they do not lose their reactivity because the surface is not reconstructed and still flexible. Low water coverage ( $3 \text{ OH nm}^{-2}$ ) has the additional effect of generating highly Lewis acidic  $\text{Al}_{\text{IV}}$  sites, which come close in reactivity to  $\text{Al}_{\text{III}}$  and therefore strongly coordinate  $\text{N}_2$ . However, in view of a volcano curve for the adsorption site density as a function of pretreatment temperature of alumina very similar to that of  $\text{CH}_4$  (which selectively adsorbs on  $\text{Al}_{\text{III}}$ ) and a single band in the IR spectrum which matches best with the value calculated for adsorption on  $\text{Al}_{\text{III}}$ , one can propose that  $\text{N}_2$  selectively coordinates to these sites. In contrast, the more basic CO molecule readily adsorbs on all types of Al sites, including those of the (100) termination, and we find similar adsorption energies and spectroscopic signatures on  $\text{Al}_{\text{III}}$  and  $\text{Al}_{\text{IV}}$  sites. These features make CO non site-specific, despite its widespread and well-accepted use as a probe for the acidity of oxide surfaces.

The adsorption of  $\text{CH}_4$  and  $\text{H}_2$  relies on the same types of Al sites that bind  $\text{N}_2$ , with the caveat that Lewis basic O sites are simultaneously involved. For  $\text{CH}_4$  and  $\text{H}_2$  the  $\text{Al}_{\text{III}}$  site, in conjunction with di- or tricoordinate O is by far the most reactive in terms of adsorption energies and barriers. As for  $\text{N}_2$ , only surfaces with low water coverage ( $3 \text{ OH nm}^{-2}$ ) are reactive because the  $\text{Al}_{\text{III}}$  sites are flexible and thus highly reactive. Moreover, adsorbed water has the additional effect of dramatically increasing the basicity of O atoms facing those sites, overall generating highly reactive "frustrated" Al<sub>2</sub>O pairs which are even more reactive than on the hypothetical, fully dehydrated (110) surface. The barrier for splitting the C–H bond is very low ( $45 \text{ kJ mol}^{-1}$  for  $\text{CH}_4$ ), and  $\text{H}_2$  dissociation is practically barrierless, thus rationalizing the reactivity of these molecules at low temperature. At low water coverage specific four-coordinate  $\text{Al}_{\text{IV}}$  sites can become potential reaction sites, in particular for  $\text{H}_2$  at high reaction temperature. This type of site can undergo reconstruction if adsorbed water is present on adjacent Al sites, yielding stable tetrahedral Al–H species similar to those formed on  $\text{Al}_{\text{III}}$ , thus preventing their distinction by spectroscopic methods. Generally speaking,  $\text{H}_2$  is always more reactive than  $\text{CH}_4$  because of its higher acidity and lower dissociation barrier. Therefore the  $\text{H}_2$  molecule will react on all  $\gamma\text{-Al}_2\text{O}_3$  (110) terminated sites, even at rather high water coverage, in particular when the reaction occurs at higher temperature. For instance  $\text{H}_2$  hence dissociates on  $\text{Al}_{\text{IVa}}$  and forms stable bridging hydrides, while  $\text{CH}_4$  is totally unreactive

on these sites. This explains the significantly higher reactive site density at a given temperature, when comparing  $\text{H}_2$  and  $\text{CH}_4$ .

Finally, pretreatment temperatures for alumina exceeding  $700 \text{ }^\circ\text{C}$  lead to a rapid decline of the number of adsorption sites for  $\text{N}_2$ ,  $\text{CH}_4$ , and  $\text{H}_2$  because  $\gamma\text{-Al}_2\text{O}_3$  is transformed to  $\theta$  and ultimately  $\alpha$ . While this phase transition is a bulk process, it is accompanied by a strong loss of surface area. In fact, the transformation of the surface most likely precedes that of the bulk, so that the surface reactivity changes faster than deduced from the bulk structure.<sup>47</sup> The reorganization of the surface (and of the bulk) at high temperatures is to be associated with the higher mobility of oxygen of  $\text{Al}_2\text{O}_3$  at high temperature<sup>78</sup> and the instability of the major (110) termination compared to other terminations, such as the minor (100), in the absence of adsorbed water.<sup>50</sup> Overall, while we do not know the exact nature of the surface transformations, we can rationalize the loss of reactivity: The  $\text{Al}_{\text{III}}$  sites, present only on the (110) termination and mainly responsible for these adsorption phenomena, disappear together with the (110) termination.<sup>79</sup>

Although such knowledge seems to be seldom exploited, the importance of the thermal pretreatment step on the performance of transition alumina based catalysts was recognized early in H–D exchange,<sup>26,35,80</sup> and the skeletal isomerization of 1-pentene<sup>81</sup> where the optimal pretreatment temperature is around  $600\text{--}700 \text{ }^\circ\text{C}$ . Moreover,  $\text{NH}_3$  adsorption<sup>82</sup> and the catalytic performance<sup>81</sup> of the  $\eta$ -polymorph show a nearly identical dependence on the pretreatment temperature, suggesting that similar  $\text{Al}_{\text{III}}$  "defects" are present. The fact that the (110) termination predominates on  $\eta\text{-Al}_2\text{O}_3$  particles,<sup>43</sup> the observation of strong  $\text{N}_2$  adsorption, leading to a single sharp band in IR,<sup>83</sup> and  $\text{H}_2$  dissociation yielding Al–H IR bands identical to those found on  $\gamma\text{-Al}_2\text{O}_3$ <sup>84</sup> are fully consistent with this proposal.

We are currently exploring such directions on alumina-based systems, which rely on "defect" sites for the generation of the active species, for example, the olefin metathesis catalyst  $\text{CH}_3\text{ReO}_3/\text{Al}_2\text{O}_3$ . Note that for the related  $\text{Re}_2\text{O}_7/\text{Al}_2\text{O}_3$  system, an optimal activation temperature of  $750 \text{ }^\circ\text{C}$  was determined.<sup>85</sup> Our findings should also have implications for alumina-supported organozirconium-<sup>11,13,86</sup> and hafnium-based<sup>87,88</sup> olefin polymerization catalysts and zirconium and tungsten hydrides active in alkane hydrogenolysis and metathesis.<sup>20,23</sup> Finally, we propose that the general concepts outlined here, i.e. the creation and stabilization of highly reactive Lewis acid–base pairs by hydration of the surface, could apply generally to (nonreducible) oxide surfaces. Further work is currently under way in that direction.

## ■ ASSOCIATED CONTENT

### 📄 Supporting Information

Detailed experimental and computational procedures, a powder XRD study of the thermal treatment of alumina, additional figures including PDOS for all surface sites discussed in the article, and tables containing TS geometries. This information is available free of charge via the Internet at <http://pubs.acs.org>

## ■ AUTHOR INFORMATION

### Corresponding Author

ccoperet@inorg.chem.ethz.ch; Philippe.Sautet@ens-lyon.fr

### Notes

The authors declare no competing financial interest.

## ■ ACKNOWLEDGMENTS

Dedicated to R. A. Andersen in honor of his 70th birthday. The authors thank IDRIS, CINES, and the ETH Zürich (Brutus cluster) for computational resources and Sasol Germany GmbH and Evonik AG for gifts of alumina. This work was in part supported by the Ministère de l'Éducation Nationale through a Ph.D. scholarship for R.W. (2007–2010).

## ■ REFERENCES

- (1) Knözinger, H.; Ratnasamy, P. *Catal. Rev. Sci. Eng.* **1978**, *17*, 31–70.
- (2) Hudson, K. L.; Misra, C.; Perrotta, A. J.; Wefers, K.; Williams, F. S. In *Ullmann's Encyclopedia of Industrial Chemistry*; Wiley-VCH: Hoboken, NJ, 2003, pp 339–378.
- (3) Wefers, K.; Misra, C. *Alcoa technical paper no. 19: The Oxides and Hydroxides of Aluminum*; 1987. See [http://www.alcoa.com/global/en/innovation/papers\\_patents/details/1987\\_paper\\_oxides\\_and\\_hydroxides.asp](http://www.alcoa.com/global/en/innovation/papers_patents/details/1987_paper_oxides_and_hydroxides.asp).
- (4) Euzen, P.; Raybaud, P.; Krokidis, X.; Toulhoat, H.; Loarer, J.-L. L.; Jolivet, J.-P.; Froidefond, C. In *Handbook of Porous Solids*; Schüth, F., Sing, K. S. W., Weitkamp, J., Eds.; Wiley: Hoboken, NJ, 2008, pp 1591–1677.
- (5) Kwak, J. H.; Hu, J.; Mei, D.; Yi, C.-W.; Kim, D. H.; Peden, C. H. F.; Allard, L. F.; Szanyi, J. *Science* **2009**, *325*, 1670–1673.
- (6) Schüth, F. *Chem. Unserer Zeit* **2006**, *40*, 92–103.
- (7) Rascon, F.; Wischert, R.; Copéret, C. *Chem. Sci.* **2011**, *2*, 1449–1456.
- (8) Ballard, D. G. H. *J. Polym. Sci., Part A: Polym. Chem.* **1975**, *13*, 2191–2212.
- (9) Burwell, R. L., Jr. *J. Catal.* **1984**, *86*, 301–314.
- (10) Dahmen, K. H.; Hedden, D.; Burwell, R. L.; Marks, T. J. *Langmuir* **1988**, *4*, 1212–1214.
- (11) Marks, T. J. *Acc. Chem. Res.* **1992**, *25*, 57–65.
- (12) Eisen, M. S.; Marks, T. J. *J. Am. Chem. Soc.* **1992**, *114*, 10358–10368.
- (13) Motta, A.; Fragalà, I. L.; Marks, T. J. *J. Am. Chem. Soc.* **2008**, *130*, 16533–16546.
- (14) Joubert, J.; Delbecq, F.; Sautet, P.; Roux, E. L.; Taoufik, M.; Thieuleux, C.; Blanc, F.; Copéret, C.; Thivolle-Cazat, J.; Basset, J.-M. *J. Am. Chem. Soc.* **2006**, *128*, 9157–9169.
- (15) Mol, J. C. *Catal. Today* **1999**, *51*, 289–299.
- (16) Salameh, A.; Copéret, C.; Basset, J.-M.; Böhm, V. P. W.; Röper, M. *Adv. Synth. Catal.* **2007**, *349*, 238–242.
- (17) Wagner, W. Ph.D. Thesis, Technische Universität München, Munich, Germany, 1990.
- (18) Salameh, A.; Joubert, J.; Baudouin, A.; Lukens, W.; Delbecq, F.; Sautet, P.; Basset, J.-M.; Copéret, C. *Angew. Chem., Int. Ed.* **2007**, *46*, 3870–3873.
- (19) Salameh, A.; Baudouin, A.; Soulivong, D.; Boehm, V.; Röper, M.; Basset, J.-M.; Copéret, C. *J. Catal.* **2008**, *253*, 180–190.
- (20) Le Roux, E.; Taoufik, M.; Copéret, C.; Mallmann, A. d.; Thivolle-Cazat, J.; Basset, J.-M.; Maunders, B. M.; Sunley, G. J. *Angew. Chem., Int. Ed.* **2005**, *44*, 6755–6758.
- (21) Basset, J.-M.; Copéret, C.; Soulivong, D.; Taoufik, M.; Cazat, J. T. *Acc. Chem. Res.* **2009**, *43*, 323–334.
- (22) Copéret, C. *Chem. Rev.* **2010**, *110*, 656–680.
- (23) Joubert, J.; Delbecq, F.; Thieuleux, C.; Taoufik, M.; Blanc, F.; Copéret, C.; Thivolle-Cazat, J.; Basset, J.-M.; Sautet, P. *Organometallics* **2007**, *26*, 3329–3335.
- (24) Ohno, S.; Yasumori, I. *Bull. Chem. Soc. Jpn.* **1968**, *41*, 2227–2233.
- (25) Van Cauwelaert, F. H.; Hall, W. K. *Trans. Faraday Soc.* **1970**, *66*, 454–468.
- (26) Holm, C. V. C. F.; Blue, R. W. *Ind. Eng. Chem.* **1951**, *43*, 501–505.
- (27) Weller, S. W.; Hindin, S. G. *J. Phys. Chem.* **1956**, *60*, 1506–1512.
- (28) Pines, H.; Ravoire, J. *J. Phys. Chem.* **1961**, *65*, 1859–1861.
- (29) Amenomiya, Y. *J. Catal.* **1971**, *22*, 109–122.
- (30) Borovkov, V. I.; Muzyka, I. S.; Kazanskii, V. B. *Dokl. Akad. Nauk SSSR* **1982**, *265*, 109–112.
- (31) Larson, J. G.; Hall, W. K. *J. Phys. Chem.* **1965**, *69*, 3080–3089.
- (32) Muzyka, I. S.; Zubkov, S. A.; Borovkov, V. I.; Kazanskii, V. B. *Dokl. Akad. Nauk SSSR* **1985**, *284*, 391–394.
- (33) Quanzhi, L.; Amenomiya, Y. *Appl. Catal.* **1986**, *23*, 173–182.
- (34) Trokhimets, A. I.; Markevich, S. V. *Russ. J. Phys. Chem.* **1965**, *39*, 1055.
- (35) Flockhart, B. D.; Uppal, S. S.; Pink, R. C. *Trans. Faraday Soc.* **1971**, *67*, 513–525.
- (36) Hightower, J. W.; Hall, W. K. *Trans. Faraday Soc.* **1970**, *66*, 477–489.
- (37) Hightower, J. W.; Saunders, P. C. *J. Phys. Chem.* **1970**, *74*, 4323–4329.
- (38) Peri, J. B. *J. Phys. Chem.* **1966**, *70*, 3168–3179.
- (39) Wischert, R.; Copéret, C.; Delbecq, F.; Sautet, P. *Chem. Commun.* **2011**, *47*, 4890–4892.
- (40) Joubert, J.; Salameh, A.; Krakoviack, V.; Delbecq, F.; Sautet, P.; Copéret, C.; Basset, J.-M. *J. Phys. Chem. B* **2006**, *110*, 23944–23950.
- (41) Wischert, R.; Copéret, C.; Delbecq, F.; Sautet, P. *Angew. Chem., Int. Ed.* **2011**, *50*, 3202–3205.
- (42) Gribov, E. N.; Zavorotynska, O.; Agostini, G.; Vitillo, J. G.; Ricchiardi, G.; Spoto, G.; Zecchina, A. *Phys. Chem. Chem. Phys.* **2010**, *12*, 6474–6482.
- (43) Reller, A.; Cocke, D. L. *Catal. Lett.* **1989**, *2*, 91–95.
- (44) Beaufils, J. P.; Barbaux, Y. *J. Chim. Phys. Phys.-Chim. Biol.* **1981**, *78*, 347–352.
- (45) Nortier, P.; Fourre, P.; Saad, A. B. M.; Saur, O.; Lavalley, J. C. *Appl. Catal.* **1990**, *61*, 141–160.
- (46) Marchese, L.; Bordiga, S.; Coluccia, S.; Martra, G.; Zecchina, A. *J. Chem. Soc., Faraday Trans.* **1993**, *89*, 3483–3489.
- (47) Kwak, J. H.; Peden, C. H. F.; Szanyi, J. *J. Phys. Chem. C* **2011**, *115*, 12575–12579.
- (48) Pellets of  $\gamma$ -Al<sub>2</sub>O<sub>3</sub> (SBa-200) were not found sufficiently transparent in the spectral region of interest.
- (49) Krokidis, X.; Raybaud, P.; Gobichon, A. E.; Rebours, B.; Euzen, P.; Toulhoat, H. *J. Phys. Chem. B* **2001**, *105*, 5121–5130.
- (50) Digne, M.; Sautet, P.; Raybaud, P.; Euzen, P.; Toulhoat, H. *J. Catal.* **2004**, *226*, 54–68.
- (51) Perdew, J. P.; Wang, Y. *Phys. Rev. B: Condens. Matter Phys.* **1992**, *45*, 13244–13249.
- (52) Kresse, G.; Furthmüller, J. *Comput. Mater. Sci.* **1996**, *6*, 15–50.
- (53) Kresse, G.; Furthmüller, J. *Phys. Rev. B: Condens. Matter Phys.* **1996**, *54*, 11169–11186.
- (54) Blöchl, P. E. *Phys. Rev. B: Condens. Matter* **1994**, *50*, 17953–17979.
- (55) Henkelman, G.; Uberuaga, B. P.; Jonsson, H. *J. Chem. Phys.* **2000**, *113*, 9901–9904.
- (56) Henkelman, G.; Jonsson, H. *J. Chem. Phys.* **2000**, *113*, 9978–9985.
- (57) Digne, M.; Sautet, P.; Raybaud, P.; Euzen, P.; Toulhoat, H. *J. Catal.* **2002**, *211*, 1–5.
- (58) Walder, R.; Franklin, J. L. *Int. J. Mass Spectrom.* **1980**, *36*, 85–112.
- (59) Bolis, V.; Cerrato, G.; Magnacca, G.; Morterra, C. *Thermochim. Acta* **1998**, *312*, 63–77.
- (60) Lavalley, J. C.; Benaissa, M. In *Studies in Surface Science and Catalysis*; Che, M., Bond, G. C., Eds.; Elsevier: Maryland Heights, MO, 1985; Vol. 21, pp 251–261.
- (61) Welch, G. C.; Juan, R. R. S.; Masuda, J. D.; Stephan, D. W. *Science* **2006**, *314*, 1124–1126.
- (62) Guo, Y.; Li, S. *Inorg. Chem.* **2008**, *47*, 6212–6219.
- (63) Stephan, D. W. *Dalton Trans.* **2009**, 3129–3136.
- (64) Luo, Y.-R. *Comprehensive Handbook of Chemical Bond Energies*; CRC Press: Boca Raton, FL, 2007.
- (65) Eisch, J. J. In *Comprehensive Organometallic Chemistry*; Wilkinson, G., Stone, F. G. A., Abel, E. W., Eds.; Pergamon: Oxford, 1982, p 555–682.

- (66) Allendorf, M. D.; Melius, C. F.; Cosic, B.; Fontijn, A. *J. Phys. Chem. A* **2002**, *106*, 2629–2640.
- (67) Wang, Z.-C.; Weiske, T.; Kretschmer, R.; Schlangen, M.; Kaupp, M.; Schwarz, H. *J. Am. Chem. Soc.* **2011**, *133*, 16930–16937.
- (68) Ma, J.-B.; Wang, Z.-C.; Schlangen, M.; He, S.-G.; Schwarz, H. *Angew. Chem., Int. Ed.* **2012**, *51*, 5991–5994.
- (69) Linstrom, J.; Mallard, W. G. *NIST Chemistry WebBook, NIST Standard Reference Database Number 69*; National Institute of Standards and Technology: Gaithersburg, MD; <http://webbook.nist.gov>.
- (70) *CRC Handbook of Chemistry and Physics*, 92th ed.; CRC Press: Boca Raton, FL, 2011–2012; <http://www.hbcpnetbase.com>.
- (71) Copéret, C.; Grouiller, A.; Basset, J. M.; Chermette, H. *ChemPhysChem* **2003**, *4*, 608–611.
- (72) Balcells, D.; Clot, E.; Eisenstein, O. *Chem. Rev.* **2010**, *110*, 749–823.
- (73) Werkema, E. L.; Maron, L.; Eisenstein, O.; Andersen, R. A. *J. Am. Chem. Soc.* **2007**, *129*, 6662–6662.
- (74) Benco, L.; Bucko, T.; Hafner, J.; Toulhoat, H. *J. Phys. Chem. B* **2005**, *109*, 20361–20369.
- (75) Hoffmann, R. *Angew. Chem., Int. Ed. Engl.* **1987**, *26*, 846–878.
- (76) Hammer, B.; Nørskov, J. K. In *Advances in Catalysis*; Bruce, C. Gates, H. K., Ed.; Academic Press/Elsevier: Maryland Heights, MO, 2000; Vol. 45, pp 71–129.
- (77) Kwak, J. H.; Mei, D.; Peden, C. H. F.; Rousseau, R.; Szanyi, J. *Catal. Lett.* **2011**, *141*, 649–655.
- (78) Martin, D.; Duprez, D. *J. Phys. Chem.* **1996**, *100*, 9429–9438.
- (79) Lodziana, Z.; Topsoe, N.-Y.; Nørskov, J. K. *Nat. Mater.* **2004**, *3*, 289–293.
- (80) Baumgarten, E.; Zachos, A. *J. Catal.* **1981**, *69*, 121–127.
- (81) MacIver, D. S.; Wilmot, W. H.; Bridges, J. M. *J. Catal.* **1964**, *3*, 502–511.
- (82) Maciver, D. S.; Tobin, H. H.; Barth, R. T. *J. Catal.* **1963**, *2*, 485–497.
- (83) Zubkov, S. A.; Borovkov, V. Y.; Gagarin, S. G.; Kazanskii, V. B. *Chem. Phys. Lett.* **1984**, *107*, 337–340.
- (84) Kazansky, V. B.; Borovkov, V. Y.; Zaitsev, A. V. In *Proceedings of the 9th International Congress on Catalysis (Calgary, Canada)*; Phillips, M. J., Ternan, M., Eds.; The Chemical Institute of Canada: Ottawa, Canada, 1988, pp 1426–1433.
- (85) Schekler-Nahama, F.; Clause, O.; Commereuc, D.; Saussey, J. *Appl. Catal., A* **1998**, *167*, 237–245.
- (86) Joubert, J.; Delbecq, F.; Copéret, C.; Basset, J.-M.; Sautet, P. *Top. Catal.* **2008**, *48*, 114–119.
- (87) Delgado, M.; Santini, C. C.; Delbecq, F.; Wischert, R.; le-Guennic, B.; Tosin, G.; Spitz, R.; Basset, J.-M.; Sautet, P. *J. Phys. Chem. C* **2010**, *114*, 18516–18528.
- (88) Delgado, M.; Delbecq, F.; Santini, C.; Lefebvre, F.; Norsic, S.; Putaj, P.; Sautet, P.; Basset, J.-M. *J. Phys. Chem. C* **2011**, *116*, 834–843.